6-5-2021

Biotransformation of doxycycline by *Brevundimonas naejangsanensis* and *Sphingobacterium mizutaii* strains

Ting He

Jianguo Bao

Yifei Leng

Daniel D. Snow

Shuqiong Kong

See next page for additional authors

Authors

Ting He, Jianguo Bao, Yifei Leng, Daniel D. Snow, Shuqiong Kong, Tong Wang, and Xu Li

Biotransformation of doxycycline by *Brevundimonas naejangsanensis* and *Sphingobacterium mizutaii* strains

Ting He,[1,2] Jianguo Bao,[1] Yifei Leng,[3] Daniel Snow,[4] Shuqiong Kong,[1] Tong Wang,[1] & Xu Li [2]

1 School of Environmental Studies, China University of Geosciences, No. 388 Lumo Road, Wuhan, Hubei 430074, China
2 Department of Civil and Environmental Engineering, University of Nebraska-Lincoln, 900 N 16th St., W150D Nebraska Hall, Lincoln, NE 68588-0531, USA
3 School of Civil Engineering, Architecture and Environment, Hubei University of Technology, Wuhan 430068, China
4 Water Sciences Laboratory, University of Nebraska-Lincoln, Lincoln, NE 68583, USA

Corresponding authors —J. Bao, bjianguo@cug.edu.cn ; X. Li, xuli@unl.edu

ORCID Xu Li 0000-0002-1006-3027

Abstract

The fate of doxycycline (DC), a second generation tetracycline antibiotic, in the environment has drawn increasing attention in recent years due to its wide usage. Little is known about the biodegradability of DC in the environment. The objective of this study was to characterize the biotransformation of DC by pure bacterial strains with respect to reaction kinetics under different environmental conditions and biotransformation products. Two bacterial strains, *Brevundimonas naejangsanensis* DD1 and *Sphingobacterium mizutaii* DD2, were isolated from chicken litter and characterized for their biotransformation capability of DC. Results show both strains rely on cometabolism to

Published in *Journal of Hazardous Materials* 411 (2021) 125126
doi:10.1016/j.jhazmat.2021.125126

Submitted 28 August 2020; revised 6 January 2021; accepted 8 January 2021; published 5 June 2021.

biotransform DC with tryptone as primary growth substrate. DD2 had higher biotransformation kinetics than DD1. The two strains prefer similar pHs (7 and 8) and temperature (30 °C), however, they exhibited opposite responses to increasing background tryptone concentration. While hydrolysis converted DC to its isomer or epimer, the two bacterial strains converted DC to various biotransformation products through a series of demethylation, dehydration, decarbonylation and deamination. Findings from the study can be used to better predict the fate of DC in the environment.

Keywords: Doxycycline, Biotransformation, Kinetic, Transformation products

1. Introduction

Doxycycline (DC) is a second generation tetracycline antibiotic synthesized by deoxygenating the C6 position of oxytetracycline (Nogueira et al., 2011; Das et al., 2019). Compared to the first generation tetracycline antibiotics, DC ($C_{22}H_{24}N_2O_8$, 444.44 g mol^{-1} (Borghi et al., 2015; Fan et al., 2019)) is a safer alternative (Heaton et al., 2007), because it is more lipid soluble (Szatmari et al., 2012) (3–5 times higher lipophilicity (Spina-Cruz et al., 2019; Agwuh and MacGowan, 2006)) and has higher bioavailability, shorter half-life, stronger antibacterial potency (Yan et al., 2018), and lower toxicity (Ponnampalam, 1981; Russell et al., 1996). Because of these traits, DC is the most commonly used tetracycline antibiotic in China (Zhang et al., 2015) and has been frequently used on livestock (Widyasari-Mehta et al., 2016) and in human medicine (Markowska et al., 2019; Grant et al., 2019). Exposure to DC could have transient effects on biomass and nitrate formation, reduce the number of earthworm juveniles, and exert negative effects on the seedling growth of tomato (Litskas et al., 2019).

With the increasing use, DC has been detected in various urban and agricultural environments (Daghrir and Drogui, 2013). For example, DC residual concentrations were 64–915 ng L^{-1} and 1.3–1.5 mg kg^{-1} in the final effluent and sludge, respectively, of municipal wastewater treatment plants in Sweden (Lindberg et al., 2005). DC was detected at 0–191 ng L^{-1} and 0–39 ng L^{-1} in reclaimed water and groundwater, respectively, in 15 cities in China (Ma et al., 2015), as well as up to 82 ng L^{-1} in surface water (Deng et al., 2016). In the Rio Grande River between the United States and Mexico, DC concentrations ranged at 76.73–130.79 ng L^{-1} in water and at 0.23–0.32 ng g^{-1} in the sediment (Fuentes et al., 2019). In agricultural environment, DC was detected at 78.5 mg kg^{-1} dry weight in

broiler chicken litter and 63–728 μg kg^{-1} in litter-amended soil following land application (Ho et al., 2014). The degradation of tetracycline antibiotics in the environmental depends on both the properties of individual antibiotic compound (e.g., water solubility, molecular structure, etc.) and the environmental conditions (e.g., soil type, light, temperature, microbial biomass, etc.) (Zaranyika et al., 2015). Tetracyclines can be removed via hydrolysis, photolysis, oxidation and biodegradation (Li and Zhang, 2010; Gothwal and Shashidhar, 2015; Dai et al., 2019). Known degradation mechanisms of DC include hydrolysis (Zaranyika et al., 2015), photocatalytic (Wang et al., 2019; Tong et al., 2019; Adamek et al., 2016; Liu et al., 2018; Bolobajev et al., 2016), adsorption (Fan et al., 2019; Liu et al., 2017, 2019; Wei et al., 2019; Chao et al., 2014; Brigante and Avena, 2016; Zhang et al., 2016), and advanced oxidation (Spina-Cruz et al., 2019; Bolobajev et al., 2016; Zhang et al., 2016). The half-lives of DC are reported to be between 4.5 days and 76.3 days under various environmental conditions (Szatmari et al., 2012; Zaranyika et al., 2015). Compared to physiochemical processes, much less is known about the biotransformation of DC. One study isolated ten DC degrading bacterial strains from a vegetable field that received manure application for years (Wen et al., 2018). It is unclear how environmental conditions affect microbial transformation of DC and what biotransformation products may form as a result of microbial activities.

The objective of this study was to characterize the biotransformation of DC by pure bacterial strains with respect to reaction kinetics under different environmental conditions and biotransformation products. In this study, two bacterial strains capable of co-metabolizing DC were isolated from soil. The biotransformation of DC by these two strains were characterized under multiple environmental conditions, such as pH, temperature, and background nutrient condition. Furthermore, the biotransformation productions of DC were characterized for the two strains, and presumptive biotransformation pathways were proposed. The use of pure cultures in this study enabled us to systematically investigate how environmental conditions may affect DC biotransformation. Because poultry facilities are a major user of DC, the pure cultures isolated from chicken litter in this study can increase our knowledge on DC biotransformation and improve our ability to predict the fate of DC in the environment such as those under the influence of DC contaminated animal wastes.

2. Materials and methods

2.1. Chemicals

Reagent grade chemicals were used in the study, Lysogeny broth (LB) medium was made of 10 g L^{-1} tryptone, 5 g L^{-1} yeast extract, and 5 g L^{-1} NaCl. LB-D solution was prepared by adding 50 mg L^{-1} DC to LB. Mineral medium (MM) was made of 1.5 g L^{-1} K_2HPO_4, 1.0 g L^{-1} NaCl, 0.5 g L^{-1} KH_2PO_4, 0.2 g L^{-1} $MgSO_4 \cdot 7H_2O$ (pH = 7.0) (Leng et al., 2016). MM-D solution was prepared by supplementing MM with 50 mg L^{-1} DC. MM-T solution was prepared by supplementing MM with 10 g L^{-1} tryptone, and MM-TD solution by supplementing MM-T with 50 mg L^{-1} DC.

2.2. Isolation and identification of degrading bacteria

Chicken litter samples were collected from a poultry facility in Henan Province, China, where DC had been used for more than 5 years. First, 0.5 g chicken feces were added into 50 mL LB-D solution. The solution was cultured at 30 °C and shaken at 150 rpm for 3 days in the dark. Then, 20 μL enriched culture was serial diluted and streaked onto MM-TD agar plates. The plates were then cultivated at 30 °C in dark for 3 days. Ten colonies with distinct shapes and colors were re-streaked on MM-TD agar plates to obtain pure cultures. Based on biotransformation performance, two bacterial strains DD1 and DD2 were selected for further analyses.

The phylogeny of DD1 and DD2 were determined using the phylogenetic analysis targeting the 16 S rRNA gene. Genomic DNA of two strains were extracted using the Genomic DNA Extraction Kit (Axygen, USA) and amplified using a PCR protocol targeting the 16S rRNA gene (Goodfellow and Stackebrandt, 1991). The PCR amplicons were purified and sequenced. The DNA sequences were searched against the GenBank database. Phylogenetic trees were built for DD1 and DD2 using ClustalX 1.8.3 with default settings.

2.3. DC biotransformation

Degradation experiments were carried out in batch reactors with 50 mL solution. Based on preliminary experiments, the following four sets of

experiments were designed: (1) different initial pH (i.e., 6.0, 7.0, 8.0, 9.0, 10.0) were conducted at 30 °C in MM-TD solutions; (2) different temperatures (i.e., 20, 25, 30, 35, 40 °C) were tested for DD1 at its optimal initial pH of 7.0 and for DD2 at its optimal initial pH of 8.0 in MM-TD solutions; (3) different concentrations of tryptone (i.e., 2, 4, 6, 8, 10 g L^{-1}) were tested with an initial pH 7.0 at 20 °C for DD1 and pH 8.0 at 30 °C for DD2 in MM-D solutions; (4) different initial DC concentrations (i.e., 20, 50, 100, 150, 200 mg L^{-1}) were tested at optimal conditions (i.e., pH 7.0, 10 g L^{-1} tryptone at 20 °C for DD1, and pH 8.0, 4 g L^{-1} tryptone at 30 °C for DD2). In all degradation experiments, 0.5 mL cell cultures (OD_{600} = 1) were added to MM-TD solution and the initial DC concentration was 50 mg L^{-1} unless noted otherwise. All experiments included triplicate degradation reactors and triplicate no-cell control reactors and were carried out in dark to prevent photo degradation.

2.4. Quantification of DC

1 mL liquid samples were periodically taken from the batch reactors and were centrifuged at 8000 g for 10 min. The supernatants were amended with McIlvaine-Na_2EDTA buffer to chelate metal ions (Wu et al., 2011), then filtered through 0.22 μm filter and stored at –20 °C. The concentration of DC was analyzed using high performance liquid chromatography (HPLC, 1220 Infinity LC, Agilent, USA) with a C18 reverse column (4.6 mm × 150 mm, 5 μm, Agilent). Chromatographic conditions: the mobile phase consisted of 0.1% oxalic acid - acetonitrile - methanol (67:22:11, v:v:v) (Cinquina et al., 2003), flow rate 1 mL min^{-1}, isocratic elution, column temperature 40 °C, injection volume 20 μL, and detection wavelength at 355 nm (Leng et al., 2016).

2.5. Identification of the transformation products

Three groups of samples were used to identify transformation products: (1) solution from the no-cell control reactors on Day 0, (2) solution from the no-cell control reactors on Day 3, and (3) solutions from the degradation reactors on Day 3. All samples were purified and concentrated using the Oasis HLB (6cc/150 mg, Waters) solid phase extraction column (Leng et al., 2016; Wu et al., 2011).

All transformation products were identified using liquid chromatography high resolution mass spectrometry (Q Exactive system, Thermo scientific, USA). C18 reverse column (4.6 mm × 150 mm, 5 μm, Agilent) was used as the chromatographic separation column with mobile phase being 0.1% formic acid solution - acetonitrile - methanol (67:22:11, v:v:v), flow rate being 0.3 mL min^{-1}, isocratic elution time being 15 min, and injection volume being 5 μL. Heated electrospray ionization (HESI) source with a spray voltage of 3.5 kV was employed and the mass spectrometry was operated under positive ion mode. S-lens RF level was set at 50%, capillary temperature at 300 °C, and collision energy at 35 eV. A full scan mode with *m/z* range of 200–600 was used for data acquisition. Xcalibur 2.1 software (Thermo Scientific) was used for mass spectra analysis. The biotransformation products of DC were proposed based on tandem quadrupole high resolution mass spectra: predicted mass (*m/z*), measured mass (*m/z*), error between predicted vs measured masses (<5 ppm), elemental composition, and intensity. Disc diffusion test was conducted on the transformation products following the protocol used in Leng et al. (2016).

2.6. Modeling

In control reactors DC reduction resulted from hydrolysis only, while in treatment reactors DC reduction resulted from both hydrolysis and biotransformation. First-order kinetics was used to describe the overall degradation process (Eq. 1) and hydrolysis process (Eq. 2) (Leng et al., 2016). The difference between Eqs. (1) and (2) accounted for the DC that was biotransformed (Eq. 3)

$$C_{HB} = C_0 - C_0 \times e^{-k_{HB} \times t} \quad (1)$$

$$C_H = C_0 - C_0 \times e^{-k_H \times t} \quad (2)$$

$$C_B = C_{HB} - C_H = C_0 \times e^{-k_H \times t} - C_0 \times e^{-k_{HB} \times t} \quad (3)$$

where C_0 is the initial concentration of DC, k_H is the first-order reaction rate constant (h^{-1}) of the hydrolysis reaction process, and k_{HB} is the first-order reaction rate constant (h^{-1}) of the overall degradation reaction (i.e., hydrolysis + biotransformation), C_H is the concentration change of DC due to hydrolysis only, C_{HB} is the concentration change of DC due to both hydrolysis and biotransformation, and C_B is the concentration change of DC due to biotransformation (mg L^{-1}).

The biotransformation of DC by DD2 was delayed for 24 h at pH 6 and 10 (Eq. 4). The biotransformation of DC by DD1 was delayed for 72 h at T = 40 °C and delayed by 24 h when tryptone concentration was 2 g L^{-1} (Eqs. 4, 5).

$$C_B = C_0 \times e^{-k_H \times (t-24)} - C_0 \times e^{-k_{HB} \times (t-24)} \quad (4)$$

$$C_B = C_0 \times e^{-k_H \times (t-72)} - C_0 \times e^{-k_{HB} \times (t-72)} \quad (5)$$

After taking the derivative on both sides of Eq. 3 over time, biotransformation rate V_B (mg L^{-1} h^{-1}, i.e., the rate of DC removal due to biotransformation) can be calculated as (Eq. 6).

$$V_B = C_0 \times (k_H \times e^{-k_H \times t} - k_{HB} \times e^{-k_{HB} \times t}) \quad (6)$$

For the experiment with different initial DC concentrations, initial biotransformation rate at time 0 was used to examine if the experimental data can be described using the Michaelis-Menten model (Eq. 7).

$$V_B = \frac{V_{B,max} \times S}{K_m + S} \quad (7)$$

where V_B is the initial biotransformation rate (h^{-1}), $V_{B,\max}$ is the maximum initial biotransformation rate (h^{-1}), K_m (mg L^{-1}) is half saturation constant, and S is the initial concentration of DC (mg L^{-1}).

3. Results

3.1. Isolation and identification of strains

Ten bacterial strains were isolated from the chicken litter. Among the ten strains, strain DD1 and DD2 exhibited faster DC biotransformation kinetics and higher DC biotransformation efficiencies over the other strains. According to the 16S rRNA gene sequence, strain DD1 and DD2 were identified as *Brevundimonas naejangsanensis* and *Sphingobacterium mizutaii* strains, respectively. The sequences of the 16S rRNA gene of the two strains have been deposited under the accession numbers MT809477 and MT809478 at GenBank. Further biotransformation studies were focused on these two strains.

3.2. Characterization of DC biotransformation

Because DC hydrolyzes in water, DC biotransformation in solution cannot be directly measured. Hence, all experiments in this study included treatment reactors that contained bacterial strain DD1 or DD2 and control reactors that contained no cells. Only hydrolysis occurred in the control reactors, while both hydrolysis and biotransformation occurred in the treatment reactors. The difference in DC concentrations between the two experiments can be attributed to biotransformation. Strain DD1 and strain DD2 could not grow in MM-D solutions (Fig. S1), suggesting that neither strain could utilize DC as the sole carbon and energy source. Therefore, an external carbon source, tryptone, was added in subsequent experiments to facilitate DC biotransformation through cometabolism.

Under optimal conditions both bacterial strains could degrade DC to very low levels. After 216 h, the residual DC concentrations in the control and the treatment reactors containing *B. naejangsanensis* strain DD1 were 37.58 mg L^{-1} and 5.20 mg L^{-1}, respectively (Fig. 1a). Similarly, after 48 h the residual DC concentrations in the control and treatment reactors containing *S. mizutaii* strain DD2 were 40.27 mg L^{-1} and 1.26 mg L^{-1}, respectively (Fig. 1b). Both hydrolysis and overall degradation can be described using first order reaction kinetics. The kinetic equations (Eqs. 1–3) described the experimental data well (Fig. 1c and d) with R^2 values ranging between 0.9826 and 0.9995. It was noticed that both strain DD1 and DD2 formed biofilm on the inner wall of the reactors. Degradation experiments with autoclaved cells show that adsorption could account for 1.2% and 1.6% reduction in DC concentrations due to adsorption by DD1 and DD2, respectively. The relatively low adsorption of DC was likely due to the surface properties and the concentrations of the pure cultures in the reactors.

An experiment was conducted to determine if strains DD1 and DD2 could utilize substrates other than tryptone for DC biotransformation through cometabolism (Fig. S2). DD1 showed some capability to biotransform DC when glucose, sucrose, or sodium acetate was used as growth substrate. DD2 was able to biotransform DC when glucose or sucrose was used as growth substrate. For both strains, tryptone appeared to perform superior or similar to the other substrates tested.

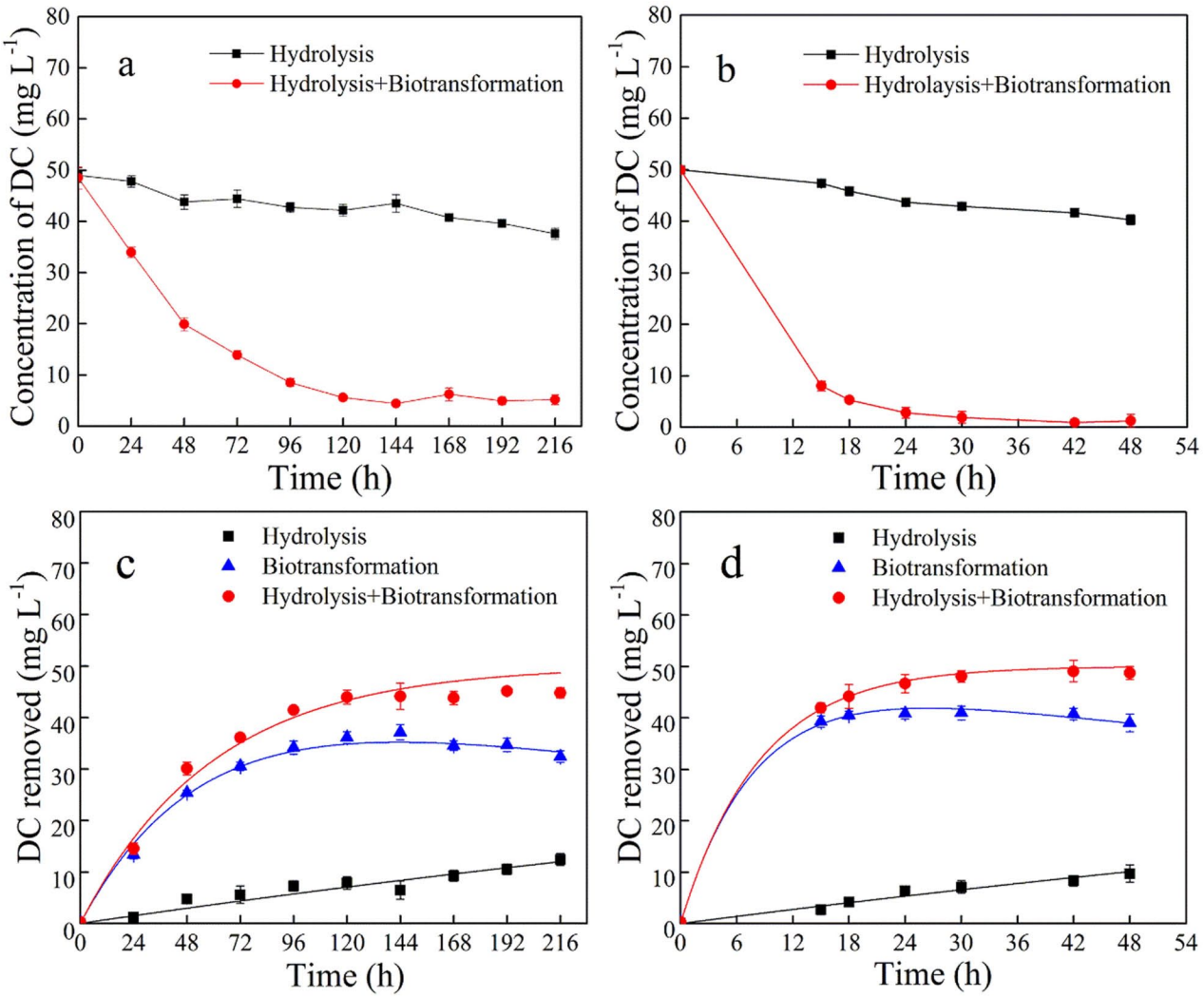

Fig. 1. The residual concentrations of DC in experiments involving strain DD1 (a) and DD2 (b) at the optimal conditions (20 °C, pH 7, 10 g L^{-1} tryptone for DD1; and 30 °C, pH 8, 4 g L^{-1} tryptone for DD2). The actual and modeled concentrations of DC removed by various mechanisms in experiments involving strain DD1 (c) and DD2 (d). Error bars represent the standard deviations from triplicate experiments. Lines were modeled using Eqs. (1)–(3). The R^2 values range between 0.9826 and 0.9970 (c), 0.9836–0.9995 (d).

3.3. Effects of pH on DC biotransformation

Both hydrolysis and biotransformation of DC were significantly affected by pH (Fig. 2). Hydrolysis rate constant k_H was positively correlated with initial pH (Fig. 2a and b inserts). For strains DD1 and DD2, the initial

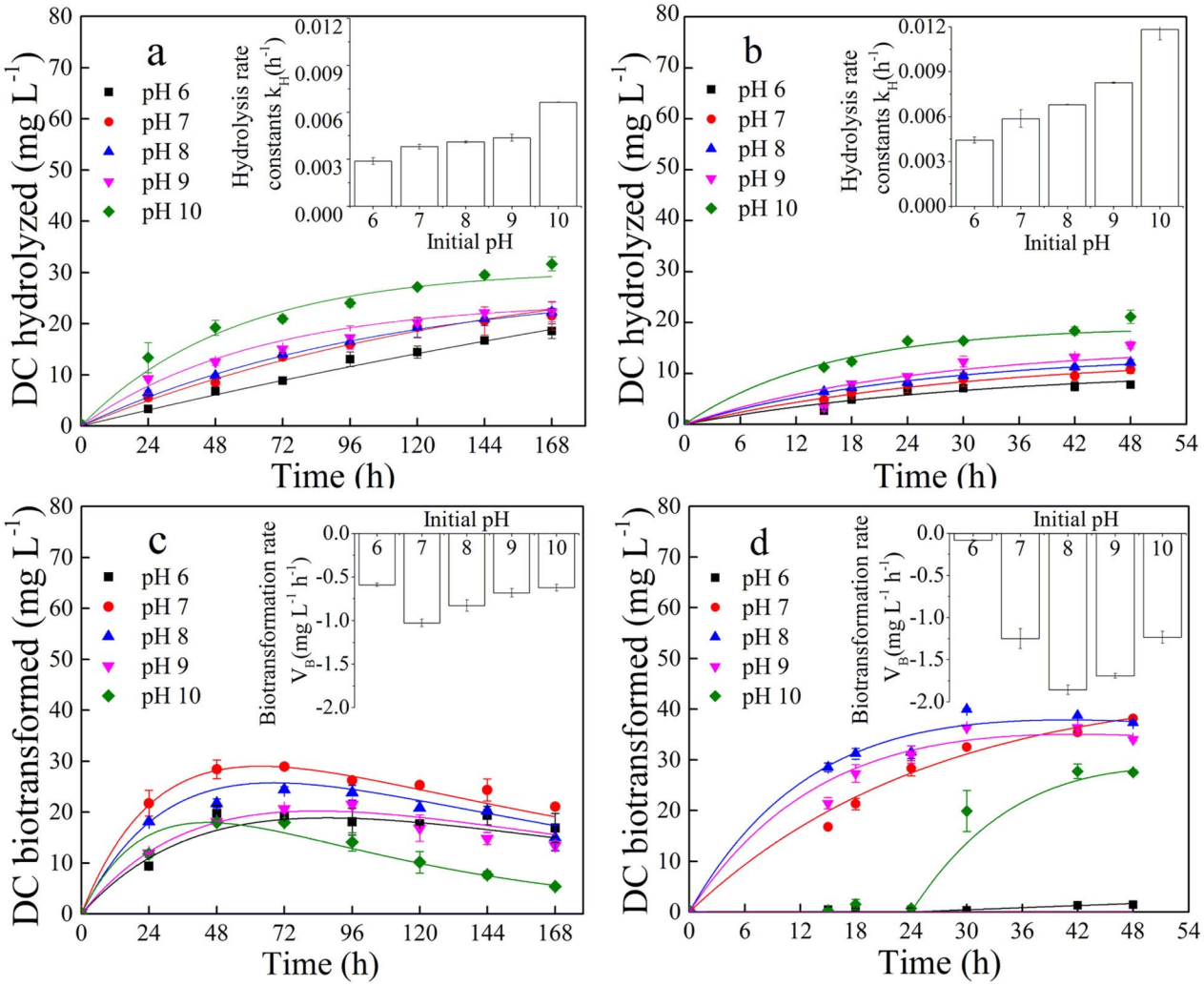

Fig. 2. The temporal changes of DC concentrations due to hydrolysis (a, b) and biotransformation (c, d) by strain DD1 (a, c) and DD2 (b, d) at different initial pHs. Lines were modeled using Eqs. (2)–(4). Error bars represent the standard deviation from triplicate experiments. The R^2 values range between 0.9903 and 0.9993 (a), 0.9107–0.9961 (b), 0.9880–0.9993 (c), 0.9788–0.9986 (d).

biotransformation rate reached the highest value at pH 7 for DD1 (V_B = 1.03 mg L^{-1} h^{-1}) and pH 8 for DD2 (V_B = 1.86 mg L^{-1} h^{-1}). At the optimal pH, a maximum of 28.92 mg L^{-1} and 39.96 mg L^{-1} DC reduction was attributed to biotransformation by DD1 and DD2, respectively (Fig. 2c and d). In addition, the biotransformation of DC by DD2 was delayed for about 24 h when the initial pH was 10. Because cells almost stopped growing under initial pH 6, there was hardly any DC biotransformation under this pH (Fig. 2d).

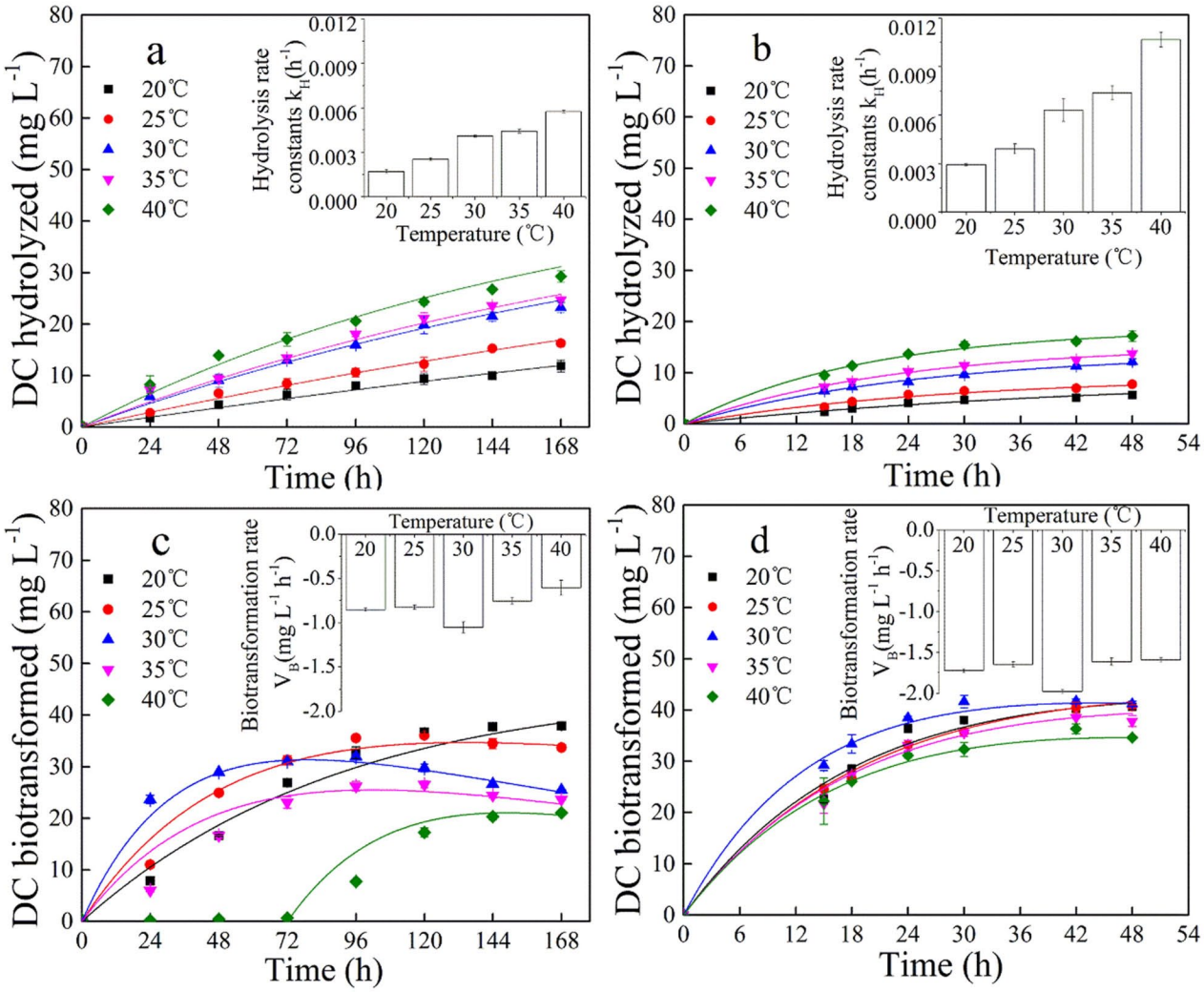

Fig. 3. The temporal changes of DC concentrations due to hydrolysis (a, b) and biotransformation (c, d) by strain DD1 (a, c) and DD2 (b, d) at different temperatures. Lines were modeled using Eqs. 2, 3 and 5. Error bars represent the standard deviation from triplicate experiments. The R^2 values range between 0.9559 and 0.9957 (a), 0.9731–0.9974 (b), 0.9592–0.9910 (c), and 0.9990–0.9998 (d).

3.4. Effects of temperature on DC biotransformation

Within the temperature range tested (20–40 °C), temperature had moderate impacts on DC biotransformation by DD1 and DD2 (Fig. 3). Hydrolysis rate constant (k_H) increased with temperature (Fig. 3a and b inserts). The highest initial biotransformation rate occurred at 30 °C for both strains with the highest biotransformation rate being 1.05 mg L^{-1} h^{-1} for DD1 and

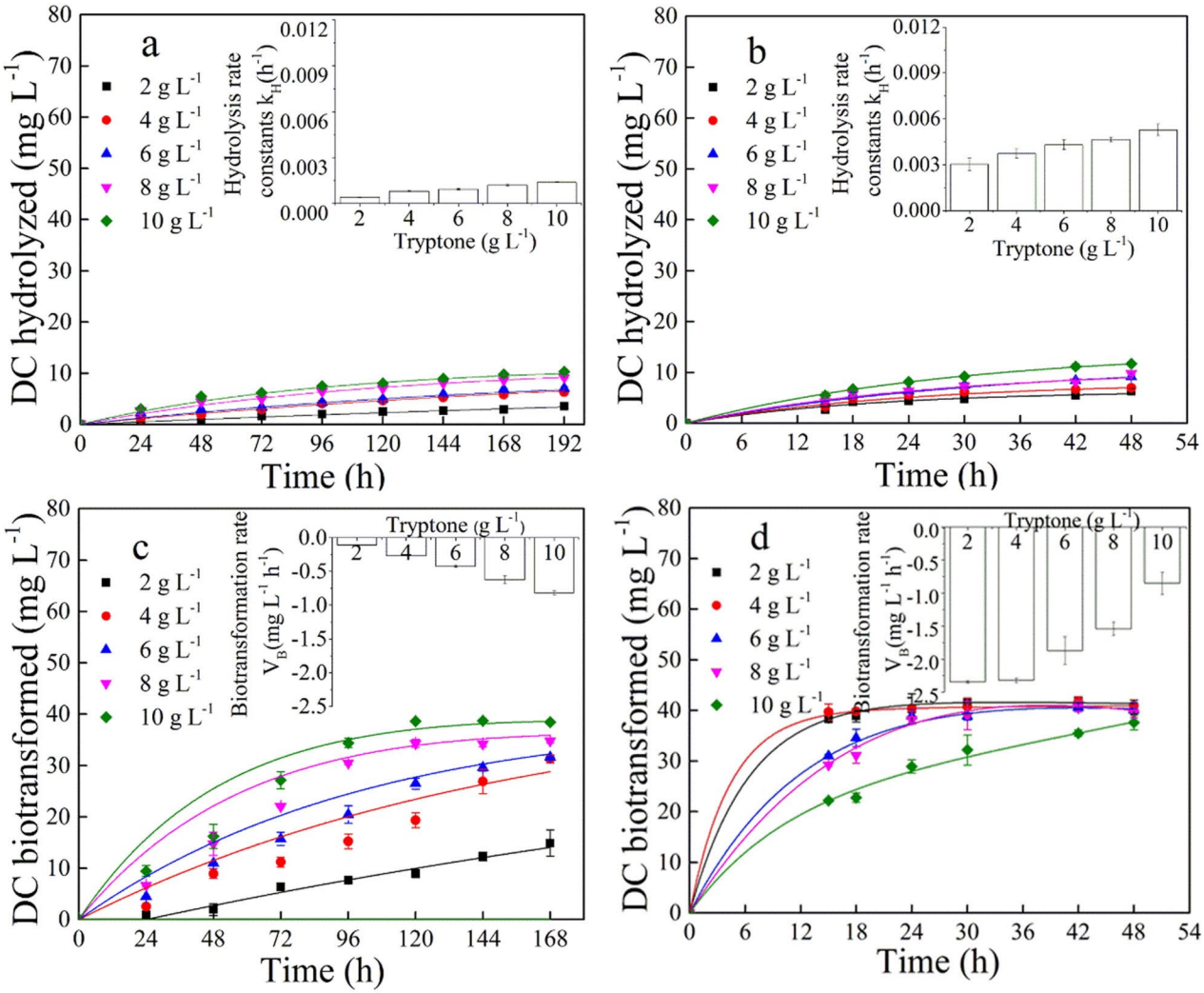

Fig. 4. The temporal changes of DC concentrations due to hydrolysis (a, b) and biotransformation (c, d) by strain DD1 (a, c) and DD2 (b, d) at different initial tryptone concentrations. Lines were modeled using Eqs. (2)–(4). Error bars represent the standard deviation from triplicate experiments. The R^2 values range between 0.9650 and 0.9963 (a), 0.9561–0.9974 (b), 0.9716–0.9890 (c), and 0.996–0.9998 (d).

1.98 mg L^{-1} h^{-1} for DD2 (Fig. 3c and d inserts). A 72-h lag phase was observed in DD1 while the temperature was set at 40 °C (Fig. 3c).

3.5. Effects of tryptone concentration on DC biotransformation

The two strains responded differently to different initial tryptone concentrations (Fig. 4). The hydrolysis rate constant increased with initial tryptone concentrations (Fig. 4a and b). For DD1, initial

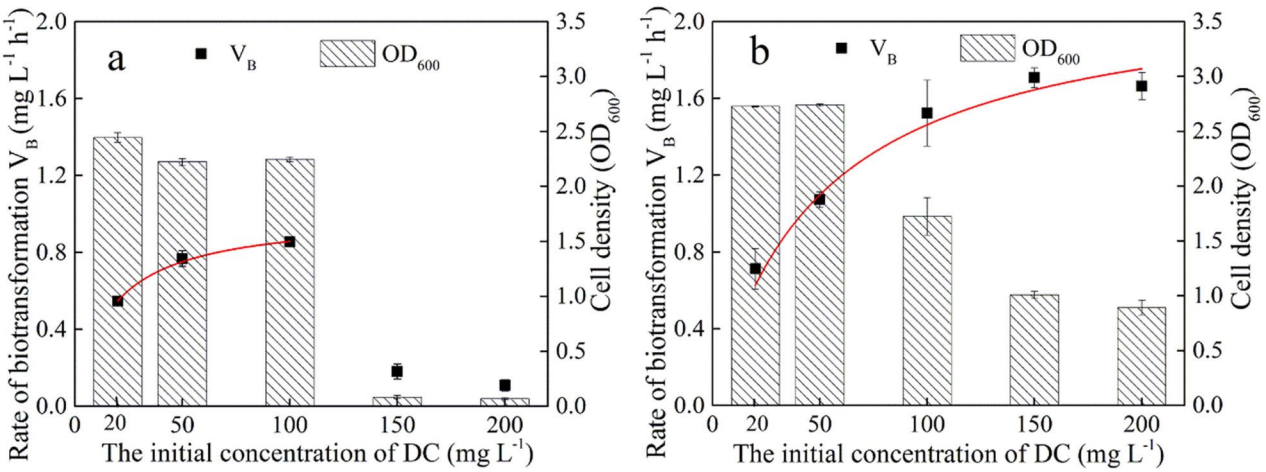

Fig. 5. The residual concentrations of DC by DD1 (a) and DD2 (b) at initial different concentration DC. Lines were modeled using Eq. (7). Error bars represent the standard deviation from triplicate experiments. The values of R^2 are 0.9669 and 0.9374.

biotransformation rate increased with initial tryptone concentrations (Fig. 4c insert). When initial tryptone concentration was 10 g L^{-1}, a maximum of 38.43 mg L^{-1} DC removal was attributed to biotransformation with an initial biotransformation rate of V_B = 0.82 mg L^{-1} h^{-1} (Fig. 4c). For strain DD2, initial biotransformation rate decreased with initial tryptone concentrations (Fig. 4d insert). When the initial tryptone concentration was 2 g L^{-1}, a maximum of 41.79 mg L^{-1} DC removal was attributed to biotransformation with an initial biotransformation rate of V_B = 2.34 mg L^{-1} h^{-1} (Fig. 4d). The biomass concentrations of DD1 and DD2 at the end of the degradation experiments conducted under different pHs, temperatures, and initial tryptone concentrations are presented in Fig. S3.

3.6. Effects of initial DC concentrations

The Michaelis-Menten model could satisfactorily describe the biotransformation kinetics of DC. For DD1, cells growth ceased when the initial DC concentrations were 150 and 200 mg L^{-1} (Fig. 5a). Non-linear regression on available data shows that $V_{B,max}$ and K_m were 1.00 mg L^{-1} h^{-1} and 16.36 mg L^{-1}, respectively, for the Michaelis-Menten equation. For DD2, cell growth was inhibited when the initial DC concentrations were 100 mg L^{-1} and above (Fig. 5b). Non-linear regression analysis on the five datum points show that $V_{B,max}$ and K_m were 2.19 mg $L^{-1}h^{-1}$ and 49.85 mg L^{-1}, respectively.

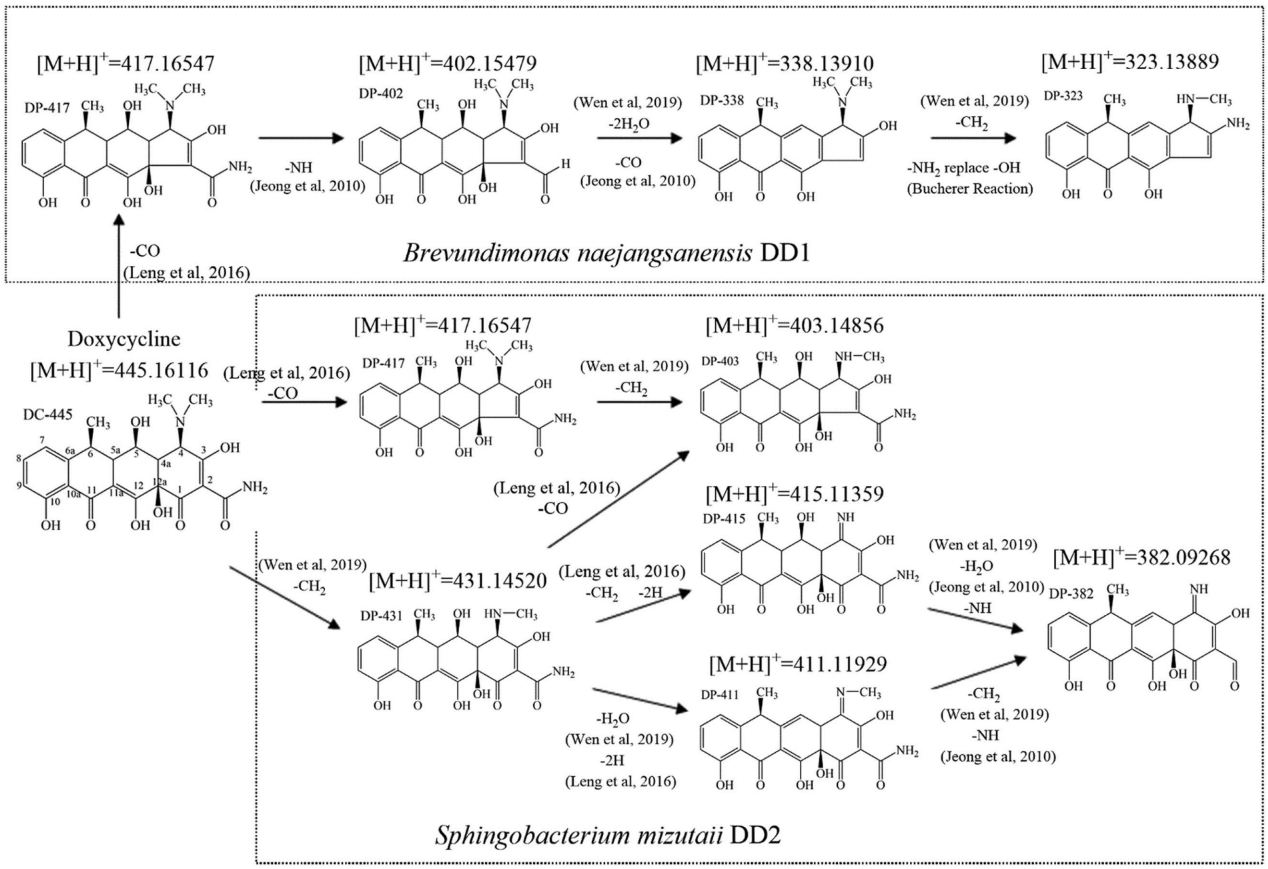

Fig. 6. The possible biotransformation pathway of DC by *B. Naejangsanensis* DD1 and *S. Mizutaii* strain DD2.

3.7. Biotransformation products

Four and six biotransformation products were tentatively identified from the biotransformation experiments with DD1 and DD2, respectively (Table 1). The mass spectra, MS-MS fragmentation profile, proposed fragmentation pattern of DC, and the biotransformation products (Fig. S4–S29) were used to support the development of the biotransformation pathways (Fig. 6). There was a peak corresponding to the epimer or isomer of DC at 0 h of the experiment (Figs. S4A and S15A) (Jutglar et al., 2018; Leng et al., 2020).

In the biotransformation of DC by strain *Brevundimonas naejangsanensis* DD1, the parent compound DC was converted to the biotransformation product DP-417 following decarbonylation at C1 (Fig. 6). After

Table1 Characteristics of the parent compound and the products from biotransformation of DC by *B. naejang*sanensis strain DD1 and *S. mizutaii* strain DD2.

Retain Time (min)	Name	Compound ion	Predicted mass (*m/z*)	Measured mass (*m/z*)	Error (ppm)	Elemental composition	Double-bond equivalents (RDB)	Intensity	MS-MS
5.88	ISO-DC or EDC	$[M+H]^+$	445.16054	445.16083	0.65	$C_{22}H_{25}O_8N_2$	11.5	2.56e + 008	428, 410
6.36	DC445	$[M+H]^+$	445.16054	445.16052	0.05	$C_{22}H_{25}O_8N_2$	11.5	6.82e + 008	428, 410
4.02	DP-417	$[M+H-CO]^+$	417.16562	417.16525	0.88	$C_{21}H_{25}O_7N_2$	10.5	1.26e + 007	400, 382
5.70	DP-402	$[M+H-CO-NH]^+$	402.15472	402.15417	1.36	$C_{21}H_{24}O_7N$	10.5	1.19e + 006	384, 366
7.62	DP-338	$[M+H-CO-NH-CO-2H_2O]^+$	338.13868	338.13910	1.24	$C_{20}H_{20}O_4N$	11.5	6.47e + 004	–
8.03	DP-323	$[M+H-CO-NH-CO-2H_2O-CH_2-OH+NH_2]^+$	323.13901	323.13889	0.37	$C_{19}H_{19}O_3N_2$	11.5	1.84e + 005	323, 277
3.31	DP-431	$[M+H-CH_2]^+$	431.14489	431.14505	0.70	$C_{21}H_{23}O_8N_2$	11.5	1.26e + 007	414, 396
4.03	DP-417	$[M+H-CO]^+$	417.16562	417.16547	0.37	$C_{21}H_{25}O_7N_2$	10.5	5.13e + 007	400, 382
3.63	DP-415	$[M+H-CH_2-CH_2]^+$	415.11359	415.11365	0.14	$C_{20}H_{19}O_8N_2$	12.5	8.84e + 007	398, 380
8.07	DP-411	$[M+H-CH_2-2-2H_2O]^+$	411.11868	411.11945	1.87	$C_{21}H_{19}O_7N_2$	13.5	2.15e + 005	366
2.52	DP-403	$[M+H-CO-CH_2]^+$	403.14998	403.14856	3.52	$C_{20}H_{23}O_7N_2$	10.5	5.26e + 005	386, 368
4.25	DP-382	$[M+H-CH_2-CH_2-2-2H_2O]^+$	382.09213	382.09265	1.36	$C_{20}H_{16}O_7N$	13.5	7.67e + 004	336

that, DP-417 went through deamination of the $O^{=}C–NH$ group outside C2 and became DP-402. DP-338 was formed by decarbonylation at the C2 position and dehydroxylation at C5 and C12a positions. DP- 338 was further converted to DP-323 by losing a methyl group from the $–N–(CH_3)_2$ group at C4 to form DP-324 (uncaptured) and by substituting the hydroxyl group of C3 with $–NH_2$.

In the biotransformation of DC by *Sphingobacterium mizutaii* DD2, the parent compound DC was biotransformed through multiple pathways. In the first pathway, DC was converted to DP-431 by losing a methyl group from the $N–(CH_3)_2$ group at C4. Further, DP-431 lost another methyl group from the $N\text{-}CH_3$ group at C4 to form DP-417 (uncaptured), which lost two hydrogen ions at C4 and became DP-415. In parallel, DP- 431 may dehydrate at C5 to form DP-413(uncaptured), which lost two hydrogen ions at C4 to form DP-411. Through these two pathways, DP- 382 may form from DP-415 through deamination of the $O^{=}C–NH_2$ group outside C2 and dehydration at C5 or from DP-411 through demethylation of the $N–CH_3$ group at C4 and deamination of the $O^{=}C–NH_2$ group outside C2. Finally, DP-403 may form from losing the carbonyl group at C1 of DP-431 or from losing the methyl group from the $N–(CH_3)_2$ group at C4 of DP-417.

3.8. Antimicrobial potency of transformation products

The biotransformation products of DD1 and DD2 exhibited lower antimicrobial potency than the parent compound DC and the products of hydrolysis (Fig. 7). For the degradation with DD1, in the control reactors where only hydrolysis occurred, residual DC decreased from 50.00 mg L^{-1} to 37.58 mg L^{-1} at 216 h and the inhibition zone decreased from 19.5 mm to 15.0 mm. In the treatment reactor where both hydrolysis and biotransformation occurred, the residual DC dropped from 50.00 mg L^{-1} to 5.20 mg L^{-1} at 216 h by DD1 and the inhibitory zone decreased from 19.4 mm to 8.3 mm. For the degradation with DD2, in the control reactors, residual DC dropped from 50.00 mg L^{-1} to 40.27 mg L^{-1} at 48 h, the inhibition zone decreased from 19.5 mm to 17.9 mm. In the treatment reactors where both hydrolysis and biotransformation occurred, the residual DC dropped from 50.00 mg L^{-1} to 1.26 mg L^{-1} at 48 h by DD2 and the inhibitory zone decreased from 19.7 mm to 9.7 mm.

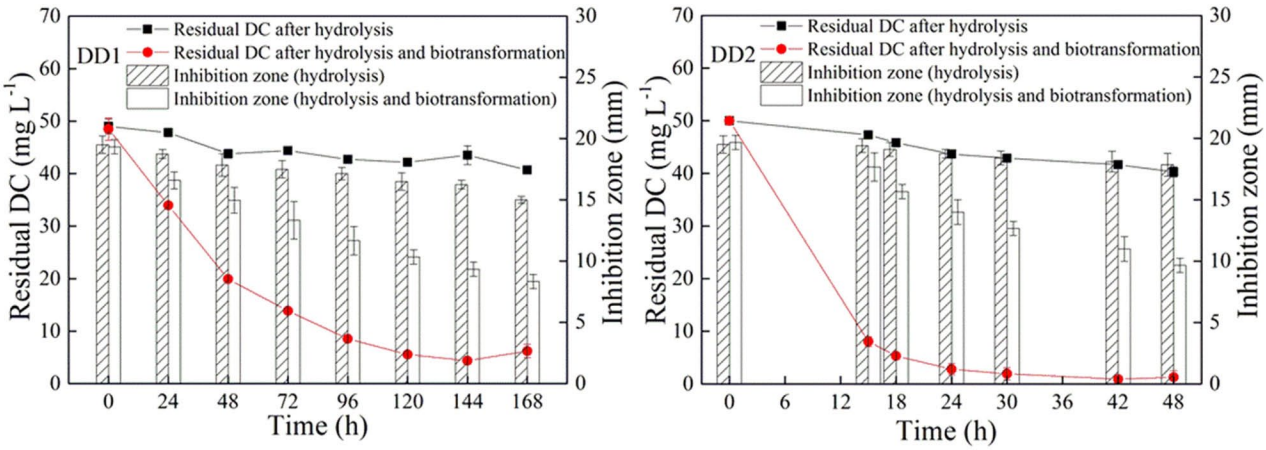

Fig. 7. The antimicrobial potency of the degradation products as measured using inhibition zones and the concentration of residual DC of DD1 at 20 °C and initial pH 7, DD2 at 30 °C and initial pH 8. The inner diameter of the wells was 6 mm in the disk diffusion test. The error bars are standard deviations from triplicate experiments.

4. Discussion

4.1. Bacterial strains

This study reports two novel bacterial strains capable of biotransforming DC, *Brevundimonas naejangsanensis* DD1 and *Sphingobacterium mizutaii* DD2. Previously, there was only one study that reported microbial degradation of DC using strains that belonged to *Ochrobactrum*, *Burkholderia*, and *Enterobacter* (Wen et al., 2018). *Brevundimonas* has been previously reported for its capability of degrading organic compounds such as antibiotic gentamicin (Liu et al., 2017) and fungicide dimethachlon (Zhang et al., 2020). Enzyme aminoglycoside 3-acetyltransferase was speculated to be responsible for the biodegradation of gentamicin in *Brevundimonas* (Liu et al., 2017). Similarly, *Sphingobacterium* also contained strains capable of degrading complex organic compounds such as phenanthrene (Son et al., 2011) and chlorpyrifos (Abraham and Silambarasan, 2013) with activities from enzymes like catechol 2,3-dioxygenase and hydrolases. *Brevundimonas naejangsanensis* sp. occurs in soil (Kang et al., 2009), while *Sphingobacterium* sp. have been isolated from soil and composts (Yoo et al., 2007; Choi and Lee, 2012).

It is worth noting that functional *tet*(X) gene has been reported in both *Sphingobacterium* and *Brevundimonas* sp. strains (Ghosh et al., 2014; Lu et al., 2019). The enzyme coded by *tet*(X) is a flavin-dependent monooxygenase, which can inactivate first and second generation tetracyclines (Ian and Moore, 2005). A recent study showed that heterologous expression of *tet*(X) gene in *E. coli* can facilitate DC biodegradation (Wen et al., 2020) by regioselectively hydroxylating the C11a of tetracycline substrate. The resulting unstable compound would then undergo non-enzymatic decomposition (Yang et al., 2004). In this study, both strains were tested positive for *tet*(X) using polymerase chain reaction (PCR), suggesting that the two strains have the genetic potential to biotransform DC using the monooxygenase coded by *tet*(X).

4.2. Effects of pH and temperature on hydrolysis and biotransformation

DC is an amphiphilic molecule with three acid dissociation constants (pKa = 3.50, 7.07, 9.13) and multiple ionizable functional groups (Bolobajev et al., 2016). There are cations, zwitterions and anions under different pH conditions. When the pH of the reaction solution increased from 6 to 10, DC mainly existed in the form of zwitterions. Different reactive species with different degrees of ionization dominate the solution and lead to different hydrolysis rates (Chao et al., 2014; Herzog et al., 2013). Biotransformation of DC by DD1 exhibited a downward trend with time (Fig. 2c). We speculate that the presence of bacterial cells interfered with hydrolysis in the treatment reactors. In other words, the hydrolysis process might have been slightly hindered by the bacterial cells in the treatment reactor, making the hydrolysis in the cell-free control reactors an overestimation of the hydrolysis in the treatment reactors. This phenomenon was also observed in an earlier study where the concentration of biotransformed tetracycline dipped slightly over time (Leng et al., 2016).

4.3. Tryptone concentration

Tetracycline antibiotics may be biotransformed by pure bacterial strains through cometabolism with tryptone (Leng et al., 2016), sucrose (Huang et al., 2016), sodium acetate (Shao et al., 2018) as primary substrates. DD1 and DD2 used tryptone as primary substrate to co-metabolize DC.

During cometabolism, catabolic enzymes degrading non-growth substrate are produced in the process of utilizing growth substrate; hence, growth substrate concentrations often affect the cometabolism of non-growth substrate (Luo et al., 2008). DD1 and DD2 responded differently to background tryptone concentration (Fig. 4). Similar studies have shown that different bacteria have different preferences for primary growth substrates. For example, when biotransforming tetracycline, *Stenotrophomonas maltophilia* DT1 had a higher biotransformation kinetics when both citrate and peptone were present as primary growth substrates than when peptone was present alone (Leng et al., 2016). The presence of glucose had an opposite effect to citrate (Leng et al., 2017). According to a kinetic model for competitive cometabolism, cometabolic transformation depends on the ratio of the initial growth to nongrowth substrate concentration and the specificity constant ratio of growth to nongrowth substrates (Kim et al., 2020). Both strains exhibited their dependence on the ratio of initial growth to nongrowth substrate (Fig. 4). The different trends between the two strains shown in Fig. 4 may be due to different specificity constant ratios of growth to nongrowth substrates. Different specificities of DD1 and DD2 for DC, a nongrowth substrate, might have determined how various initial concentrations of tryptone, a growth substrate, influence the amounts of reducing power (i.e., the NADH needed for the oxidation of both growth and nongrowth substrates when enzyme catalyzed reactions require molecular O_2 as the terminal electron acceptor) diverted to DC oxidation.

4.4. Transformation products

Because the tetracycline compounds share similar structure, they share similarity in their transformation pathways (Leng et al., 2016; Liu et al., 2016). Between pH 6.5 and pH 9, during hydrolysis the decrease in DC concentration was primarily due to conversion of DC to its isomer or epimer with no other transformation products formed (Fig. S4A, S15A). In contrast, biotransformation products were formed in the presence of DD1 and DD2. Some biotransformation processes observed in this study were similar to those observed in the biotransformation of other tetracycline compounds. For example, the demethylation reaction of the N-$(CH_3)_2$ group at C4 and the decarbonylation reaction at C1 were also reported in a study where tetracycline was transformed by horseradish

peroxidase (Leng et al., 2020). In the degradation of oxytetracycline, an α-cleavage occurs at the C1-C12a bond, forming a diradical intermediate. The resulting diradical intermediate then loses a carbonyl group and forms another diradical, which closes the ring (Liu et al., 2016). Similar transformation steps have been reported for tetracycline biotransformation by a *Stenotrophomonas maltophilia* strain (Leng et al., 2016).

The loss of the amide group from C2 (Fig. 6) also occurs during the biotransformation of tetracycline by *S. maltophilia* (Leng et al., 2016), by the gut microbiota in black soldier flies (Cai et al., 2018), and by biocatalyst laccase(de Cazes et al., 2014). This step was also proposed for tetracycline transformation by advanced oxidation (Jeong et al., 2010). The phenomenon of demethylation at C4 was also observed in tetracycline transformation by manganese oxide (Chen and Huang, 2011), laccase (Yang et al., 2017), and *S. maltophilia* (Leng et al., 2016). The loss of –2 H at C4 to form $C^{=}N$ also occurs during chloramination (Wan et al., 2013) and biotransformation of the tetracycline compound (Leng et al., 2016).

DC differs in structure from tetracycline on the position of a hydroxyl group (C5 of DC and C6 of tetracycline). Hence, reactions that happens to the hydroxyl group on tetracycline cannot be transferred to DC. One study reports that the hydroxyl group on C5 and the hydroxyl group on C12a of DC may be lost in sequence through photocatalyst Ag/AgCl-Cd-MoO_4 before a benzene ring is formed as a result of photocatalytic reaction (Wen et al., 2019).

5. Conclusions

In this study, *B. naejangsanensis* DD1and *S. Mizutaii* DD2 were characterized for their abilities to biotransform DC via cometabolism. The biotransformation kinetics were successfully modeled using a combination of first-order kinetics. The effects of pH and temperature on the biotransformation kinetics were characterized. The two strains exhibited opposite trends in their DC biotransformation kinetics in response to increasing background tryptone concentrations. Finally, the biotransformation pathways of DC by the two strains were proposed. Through a series of demethylation, dehydration, and deamination, DC was converted to degradation products DP-323 and DP-382. The results from this study advanced our knowledge on DC biodegradability and generate qualitative and quantitative information of DC biotransformation.

CRediT authorship contribution

Ting He: Investigation, Data Curation, Visualization, Writing - original draft.
Jianguo Bao: Conceptualization, Methodology, Writing - original draft, Supervision, Funding Acquisition.
Yifei Leng: Formal Analyses, Writing - review & editing.
Daniel Snow: Formal Analyses.
Shuqiong Kong: Investigation.
Tong Wang: Investigation.
Xu Li: Conceptualization, Methodology, Writing - review & editing, Supervision, Funding acquisition.

Competing Interests The authors declare that they have no known competing financial interests or personal relationships that could have appeared to influence the work reported in this paper.

Acknowledgments The authors would like to thank the financial support from the National Natural Science Foundation of China (41373083) and the National Science Foundation (1351676 and 1805990).

Appendix A. Supporting information Supplementary data associated with this article can be found in the appendix following the References.

References

Abraham, J., Silambarasan, S., 2013. Biodegradation of chlorpyrifos and its hydrolyzing metabolite 3,5,6-trichloro-2-pyridinol by *Sphingobacterium* sp. JAS3. Process Biochem. 48, 1559–1564.

Adamek, E., Baran, W., Sobczak, A., 2016. Photocatalytic degradation of veterinary antibiotics: biodegradability and antimicrobial activity of intermediates. Process Saf. Environ. Prot. 103, 1–9.

Agwuh, K.N., MacGowan, A., 2006. Pharmacokinetics and pharmacodynamics of the tetracyclines including glycylcyclines. J. Antimicrob. Chemother. 58, 256–265.

Bolobajev, J., Trapido, M., Goi, A., 2016. Effect of iron ion on doxycycline photocatalytic and Fenton-based autocatatalytic decomposition. Chemosphere 153, 220–226.

Borghi, A.A., Silva, M.F., Al Arni, S., Converti, A., Palma, M.S.A., 2015. Doxycycline degradation by the oxidative Fenton process. J. Chem. 2015, 1–9.

Brigante, M., Avena, M., 2016. Biotemplated synthesis of mesoporous silica for doxycycline removal. Effect of pH, temperature, ionic strength and Ca^{2+} concentration on the adsorption behaviour. Microporous Mesoporous Mater. 225, 534–542.

Cai, M., Ma, S., Hu, R., Tomberlin, J.K., Yu, C., Huang, Y., Zhan, S., Li, W., Zheng, L., Yu, Z., Zhang, J., 2018. Systematic characterization and proposed pathway of tetracycline degradation in solid waste treatment by *Hermetia illucens* with intestinal microbiota. Environ. Pollut. 242, 634–642.

de Cazes, M., Belleville, M.P., Petit, E., Llorca, M., Rodríguez-Mozaz, S., de Gunzburg, J., Barceló, D., Sanchez-Marcano, J., 2014. Design and optimization of an enzymatic membrane reactor for tetracycline degradation. Catal. Today 236, 146–152.

Chao, Y., Zhu, W., Wu, X., Hou, F., Xun, S., Wu, P., Ji, H., Xu, H., Li, H., 2014. Application of graphene-like layered molybdenum disulfide and its excellent adsorption behavior for doxycycline antibiotic. Chem. Eng. J. 243, 60–67.

Chen, W.R., Huang, C.H., 2011. Transformation kinetics and pathways of tetracycline antibiotics with manganese oxide. Environ. Pollut. 159, 1092–1100.

Choi, H.A., Lee, S.S., 2012. *Sphingobacterium kyonggiense* sp. nov., isolated from chloroethene-contaminated soil, and emended descriptions of *Sphingobacterium daejeonense* and *Sphingobacterium mizutaii.* Int J. Syst. Evol. Microbiol. 62, 2559–2564.

Cinquina, A.L., Longo, F., Anastasi, G., Giannetti, L., Cozzani, R., 2003. Validation of a high-performance liquid chromatography method for the determination of oxytetracycline, tetracycline, chlortetracycline and doxycycline in bovine milk and muscle. J. Chromatogr. A 987, 227–233.

Daghrir, R., Drogui, P., 2013. Tetracycline antibiotics in the environment: a review. Environ. Chem. Lett. 11, 209–227.

Dai, Y., Liu, M., Li, J., Yang, S., Sun, Y., Sun, Q., Wang, W., Lu, L., Zhang, K., Xu, J., Zheng, W., Hu, Z., Yang, Y., Gao, Y., Liu, Z., 2019. A review on pollution situation and treatment methods of tetracycline in groundwater. Sep. Sci. Technol. 55, 1005–1021.

Das, S., Faysal, M.N.A., Ferdous, J., Sachi, S., Islam, M.S., Sikder, M.H., 2019. Detection of oxytetracycline and doxycycline residue in different growth stages of commercial broiler. Bangladesh J. Vet. Med. 17, 7–14.

Deng, W., Li, N., Zheng, H., Lin, H., 2016. Occurrence and risk assessment of antibiotics in river water in Hong Kong. Ecotoxicol. Environ. Saf. 125, 121–127.

Fan, Y., Zheng, C., Hou, H., 2019. Preparation of granular activated carbon and its mechanism in the removal of isoniazid, sulfamethoxazole, thiamphenicol, and doxycycline from aqueous solution. Environ. Eng. Sci. 36, 1027–1040.

Fuentes, Maria D., Gutierrez, Stephanie, Sahagun, Daniella, Gomez, Jose, Mendoza, Jose, Ellis, Cameron C., Bauer, Stephanie, Blattner, Jonathan, Lee, Wen-Yee, Alvarez, Maria, Domínguez, D.C., 2019. Assessment of antibiotic levels, multi-drug resistant bacteria and genetic biomarkers in the waters of the Rio Grande River between the United States-Mexico border. J. Health Pollut. 9, 1–13.

Ghosh, S., LaPara, T.M., Sadowsky, M.J., 2014. Draft genome sequence of *Sphingobacterium* sp. strain PM2-P1-29, a tetracycline-degrading tetx-expressing aerobic bacterium isolated from agricultural soil. Genome Announc. 2.

Goodfellow, M., Stackebrandt, E., 1991. Nucleic Acid Techniques in Bacterialsystematics. John Wiley & Sons, pp. 115–143.

Gothwal, R., Shashidhar, T., 2015. Antibiotic pollution in the environment: a review. Clean - Soil Air Water 43, 479–489.

Grant, J.S., Stafylis, C., Celum, C., Grennan, T., Haire, B., Kaldor, J., Luetkemeyer, A.F., Saunders, J.M., Molina, J.-M., Klausner, J.D., 2019. Doxycycline prophylaxis for bacterial sexually transmitted infections. Clin. Infect. Dis. 70, 1247–1253.

Heaton, P.C., Fenwick, S.R., Brewer, D.E., 2007. Association between tetracycline or doxycycline and hepatotoxicity - a population based case–control study 1. J. Clin. Pharm. Ther. 32, 483–487.

Herzog, B., Huber, B., Lemmer, H., Horn, H., Müller, E., 2013. Analysis and *in situ* characterization of activated sludge communities capable of benzotriazole biodegradation. Environ. Sci. Eur. 25, 1–8.

Ho, Y.B., Zakaria, M.P., Latif, P.A., Saari, N., 2014. Occurrence of veterinary antibiotics and progesterone in broiler manure and agricultural soil in Malaysia. Sci. Total Environ. 488–489, 261–267.

Huang, X., Zhang, X., Feng, F., Xu, X., 2016. Biodegradation of tetracycline by the yeast strain *Trichosporon mycotoxinivorans* XPY-10. Prep. Biochem. Biotechnol. 46, 15–22.

Jeong, J., Song, W., Cooper, W.J., Jung, J., Greaves, J., 2010. Degradation of tetracycline antibiotics: mechanisms and kinetic studies for advanced oxidation/reduction processes. Chemosphere 78, 533–540.

Jutglar, M., Foradada, M., Caballero, F., Hoogmartens, J., Adams, E., 2018. Influence of the solvent system on the stability of doxycycline solutions. J. Pharm. Biomed. Anal. 159, 60–65.

Kang, S.J., Choi, N.S., Choi, J.H., Lee, J.S., Yoon, J.H., Song, J.J., 2009. *Brevundimonas naejangsanensis* sp. nov., a proteolytic bacterium isolated from soil, and reclassification of *Mycoplana bullata* into the genus *Brevundimonas* as *Brevundimonas bullata* comb. nov. Int J. Syst. Evol. Microbiol. 59, 3155–3160.

Kim, M.H., Fan, C., Pan, S.-Y., Lee, I., Lin, Y., Kim, H., 2020. Kinetics of competitive co-metabolism under aerobic conditions. Water-Energy Nexus 3, 62–70.

Leng, Y., Bao, J., Chang, G., Zheng, H., Li, X., Du, J., Snow, D., Li, X., 2016. Biotransformation of tetracycline by a novel bacterial strain *Stenotrophomonas maltophilia* DT1. J. Hazard. Mater. 318, 125–133.

Leng, Y., Bao, J., Song, D., Li, J., Ye, M., Li, X., 2017. Background nutrients affect the biotransformation of tetracycline by *Stenotrophomonas maltophilia* as revealed by genomics and proteomics. Environ. Sci. Technol. 51, 10476–10484.

Leng, Y., Bao, J., Xiao, H., Song, D., Du, J., Mohapatra, S., Werner, D., Wang, J., 2020. Transformation mechanisms of tetracycline by horseradish peroxidase with/without redox mediator ABTS for variable water chemistry. Chemosphere 258, 127306.

Li, B., Zhang, T., 2010. Biodegradation and adsorption of antibiotics in the activated sludge process. Environ. Sci. Technol. 44, 3468–3473.

Lindberg, R.H., Wennberg, P., Johansson, M.I., Tysklind, M., Andersson, B.A.V., 2005. Screening of human antibiotic substances and determination of weekly mass flows in five sewage treatment plants in Sweden. Environ. Sci. Technol. 39, 3421–3429.

Litskas, Vassilis D., Karamanlis, Xanthippos N., Prousali, Sophia P., Koveos, D.S., 2019. The xenobiotic doxycycline affects nitrogen transformations in soil and impacts earthworms and cultivated plants. J. Environ. Sci. Health A: Toxic Hazard. Subst. Environ. Eng. 54, 1441–1447.

Liu, S., Xu, W.H., Liu, Y.G., Tan, X.F., Zeng, G.M., Li, X., Liang, J., Zhou, Z., Yan, Z.L., Cai, X.X., 2017. Facile synthesis of Cu(II) impregnated biochar with enhanced adsorption activity for the removal of doxycycline hydrochloride from water. Sci. Total Environ. 592, 546–553.

Liu, S., Liu, Y., Tan, X., Liu, S., Li, M., Liu, N., Yin, Z., Tian, S., Zhou, Y., 2019. Facile synthesis of MnOx-loaded biochar for the removal of doxycycline hydrochloride: effects of ambient conditions and co-existing heavy metals. J. Chem. Technol. Biotechnol. 94, 2187–2197.

Liu, W., Zhou, J., Zhou, J., 2018. Facile fabrication of multi-walled carbon nanotubes (MWCNTs)/α-Bi_2O_3 nanosheets composite with enhanced photocatalytic activity for doxycycline degradation under visible light irradiation. J. Mater. Sci. 54, 3294–3308.

Liu, Y., He, X., Fu, Y., Dionysiou, D.D., 2016. Degradation kinetics and mechanism of oxytetracycline by hydroxyl radical-based advanced oxidation processes. Chem. Eng. J. 284, 1317–1327.

Liu, Y., Chang, H., Li, Z., Feng, Y., Cheng, D., Xue, J., 2017. Biodegradation of gentamicin by bacterial consortia AMQD4 in synthetic medium and raw gentamicin sewage. Sci. Rep. 7, 11004.

Lu, J., Zhang, Y., Wu, J., Wang, J., Zhang, C., Lin, Y., 2019. Occurrence and spatial distribution of antibiotic resistance genes in the Bohai Sea and Yellow Sea areas, China. Environ. Pollut. 252, 450–460.

Luo, W., Zhao, Y., Ding, H., Lin, X., Zheng, H., 2008. Co-metabolic degradation of bensulfuron-methyl in laboratory conditions. J. Hazard. Mater. 158, 208–214.

Ma, Y., Li, M., Wu, M., Li, Z., Liu, X., 2015. Occurrences and regional distributions of 20 antibiotics in water bodies during groundwater recharge. Sci. Total Environ. 518–519, 498–506.

Markowska, A., Kaysiewicz, J., Markowska, J., Huczyński, A., 2019. Doxycycline, salinomycin, monensin and ivermectin repositioned as cancer drugs. Bioorg. Med. Chem. Lett. 29, 1549–1554.

Moore, I.F., Hughes, D.W., Wright, G.D., 2005. Tigecycline is modified by the flavin-dependent monooxygenase TetX. Biochemistry 44, 11829–11835.

Nogueira, C.R., Damasceno, F.M., de Aquino-Neto, M.R., de Andrade, G.M., Fontenele, J. B., de Medeiros, T.A., Viana, G.S., 2011. Doxycycline protects against pilocarpine-induced convulsions in rats, through its antioxidant effect and modulation of brain amino acids. Pharmacol. Biochem. Behav. 98, 525–532.

Ponnampalam, J.T., 1981. Doxycycline in the treatment of falciparum malaria among aborigine children in West Malaysia. Trans. R. Soc. Trop. Med. Hyg. 75, 372–378.

Russell, S.M.E.P., Bell, D.L., Mancbee, R.J., Titball, R.W., 1996. Doxycycline or ciprofloxacin prophylaxis and therapy against experimental. J. Antimicrob. Chemother. 37, 769–774.

Shao, S., Hu, Y., Cheng, J., Chen, Y., 2018. Degradation of oxytetracycline (OTC) and nitrogen conversion characteristics using a novel strain. Chem. Eng. J. 354, 758–766.

Son, S.-W., Chang, H.-W., Kim, S.-K., Chang, J.-S., 2011. *Sphingobacterium* sp. SW-09 effectively degrades phenanthrene, a polycyclic aromatic hydrocarbon, in a soil microcosm. J. Life Sci. 21, 1511–1517.

Spina-Cruz, M., Maniero, M.G., Guimaraes, J.R., 2019. Advanced oxidation processes on doxycycline degradation: monitoring of antimicrobial activity and toxicity. Environ. Sci. Pollut. Res. Int. 26, 27604–27619.

Szatmari, I., Barcza, T., Kormoczy, P.S., Laczay, P., 2012. Ecotoxicological assessment of doxycycline in soil. J. Environ. Sci. Health B 47, 129–135.

Tong, Y., Kang, J., Shen, J., Chen, Z., Zhao, S., Sun, L., Wang, W., 2019. Effective degradation of doxycycline by photocatalytic $BiVO_4$–H_2O_2 under visible light. Environ. Progress Sustain. 38.

Wan, Y., Jia, A., Zhu, Z., Hu, J., 2013. Transformation of tetracycline during chloramination: kinetics, products and pathways. Chemosphere 90, 1427–1434.

Wang, W., Han, Q., Zhu, Z., Zhang, L., Zhong, S., Liu, B., 2019. Enhanced photocatalytic degradation performance of organic contaminants by heterojunction photocatalyst $BiVO_4$/TiO_2/RGO and its compatibility on four different tetracycline antibiotics. Adv. Powder Technol. 30, 1882–1896.

Wei, J., Liu, Y., Li, J., Zhu, Y., Yu, H., Peng, Y., 2019. Adsorption and co-adsorption of tetracycline and doxycycline by one-step synthesized iron loaded sludge biochar. Chemosphere 236, 124254.

Wen, X., Wang, Y., Zou, Y., Ma, B., Wu, Y., 2018. No evidential correlation between veterinary antibiotic degradation ability and resistance genes in microorganisms during the biodegradation of doxycycline. Ecotoxicol. Environ. Saf. 147, 759–766.

Wen, X., Shen, C., Niu, C., Lai, D., Zhu, M., Sun, J., Hu, Y., Fei, Z., 2019. Attachment of Ag/AgCl nanoparticles on $CdMoO_4$ microspheres for effective degradation of doxycycline under visible light irradiation: degradation pathways and mineralization activity. J. Mol. Liq. 288, 111063.

Wen, X., Huang, J., Cao, J., Xu, J., Mi, J., Wang, Y., Ma, B., Zou, Y., Liao, X., Liang, J.B., Wu, Y., 2020. Heterologous expression of the tetracycline resistance gene tetX to enhance degradability and safety in doxycycline degradation. Ecotoxicol. Environ. Saf. 191, 110214.

Widyasari-Mehta, A., Suwito, H.R., Kreuzig, R., 2016. Laboratory testing on the removal of the veterinary antibiotic doxycycline during long-term liquid pig manure and digestate storage. Chemosphere 149, 154–160.

Wu, X., Wei, Y., Zheng, J., Zhao, X., Zhong, W., 2011. The behavior of tetracyclines and their degradation products during swine manure composting. Bioresour. Technol. 102, 5924–5931.

Yan, Q., Li, X., Ma, B., Zou, Y., Wang, Y., Liao, X., Liang, J., Mi, J., Wu, Y., 2018. Different concentrations of doxycycline in swine manure affect the microbiome and degradation of doxycycline residue in soil. Front. Microbiol. 9, 3129.

Yang, J., Lin, Y., Yang, X., Ng, T.B., Ye, X., Lin, J., 2017. Degradation of tetracycline by immobilized laccase and the proposed transformation pathway. J. Hazard. Mater. 322, 525–531.

Yang, W., Moore, I.F., Koteva, K.P., Bareich, D.C., Hughes, D.W., Wright, G.D., 2004. TetX is a flavin-dependent monooxygenase conferring resistance to tetracycline antibiotics. J. Biol. Chem. 279, 52346–52352.

Yoo, S.H., Weon, H.Y., Jang, H.B., Kim, B.Y., Kwon, S.W., Go, S.J., Stackebrandt, E., 2007. *Sphingobacterium composti* sp. nov., isolated from cotton-waste composts. Int. J. Syst. Evol. Microbiol. 57, 1590–1593.

Zaranyika, M.F., Dzomba, P., Kugara, J., 2015. Speciation and persistence of doxycycline in the aquatic environment: characterization in terms of steady state kinetics. J. Environ. Sci. Health B 50, 908–918.

Zhang, C., Li, J., An, H., Wu, X., Wu, Y., Long, Y., Li, R., Xing, D., 2020. Enhanced elimination of dimethachlon from soils using a novel strain *Brevundimonas naejangsanensis* J3. J. Environ. Manag. 255, 109848.

Zhang, Q.Q., Ying, G.G., Pan, C.G., Liu, Y.S., Zhao, J.L., 2015. Comprehensive evaluation of antibiotics emission and fate in the river basins of China: source analysis, multimedia modeling, and linkage to bacterial resistance. Environ. Sci. Technol. 49, 6772–6782.

Zhang, X., Bai, B., Li Puma, G., Wang, H., Suo, Y., 2016. Novel sea buckthorn biocarbon SBC@β-FeOOH composites: efficient removal of doxycycline in aqueous solution in a fixed-bed through synergistic adsorption and heterogeneous Fenton-like reaction. Chem. Eng. J. 284, 698–707.

Supplementary Materials

Biotransformation of Doxycycline by *Brevundimonas naejangsanensis* and *Sphingobacterium mizutaii* strains

Ting He,[a,b] Jianguo Bao,[a,*] Yifei Leng,[c] Daniel Snow,[d] Shuqiong Kong,[a] Tong Wang,[a] and Xu Li[b,*]

[a] School of Environmental Studies, China University of Geosciences, Wuhan 430074, China

[b] Department of Civil and Environmental Engineering, University of Nebraska-Lincoln, Lincoln, NE, 68588, USA

[c] School of Civil Engineering, Architecture and Environment, Hubei University of Technology, Wuhan 430068, China

[d] Water Sciences Laboratory, University of Nebraska-Lincoln, Lincoln, NE, 68583, USA

Corresponding authors:

Xu Li
900 N 16th St., W150D Nebraska Hall
Lincoln, NE 68588-0531
xuli@unl.edu
(402) 472-6042

Jianguo Bao
No. 388 Lumo Road
Wuhan, Hubei Province
P. R. China 430074
bjianguo@cug.edu.cn
(027) 67883470

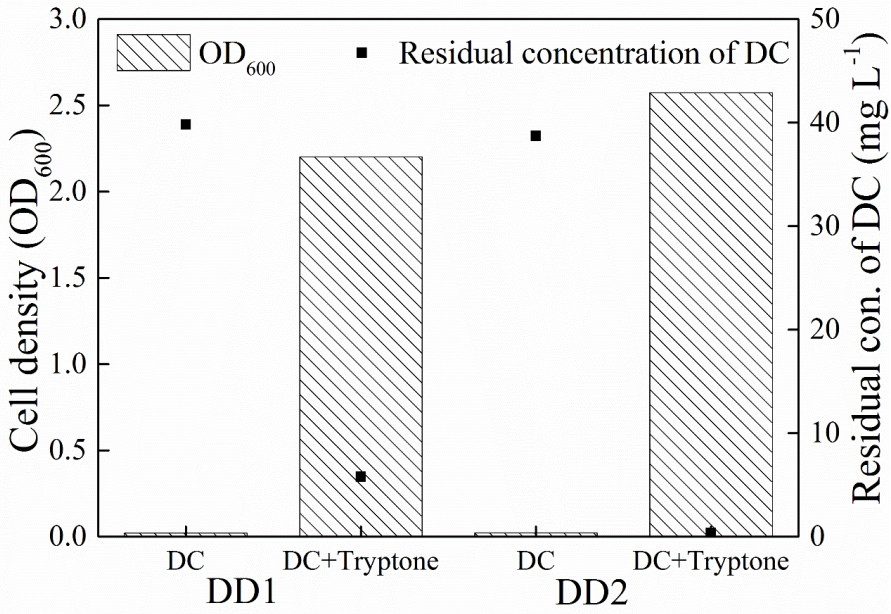

Figure S1. Neither DD1 nor DD2 could utilize DC as sole energy and carbon source. Residual DC concentrations were measured 48 hours after the start of the experiment.

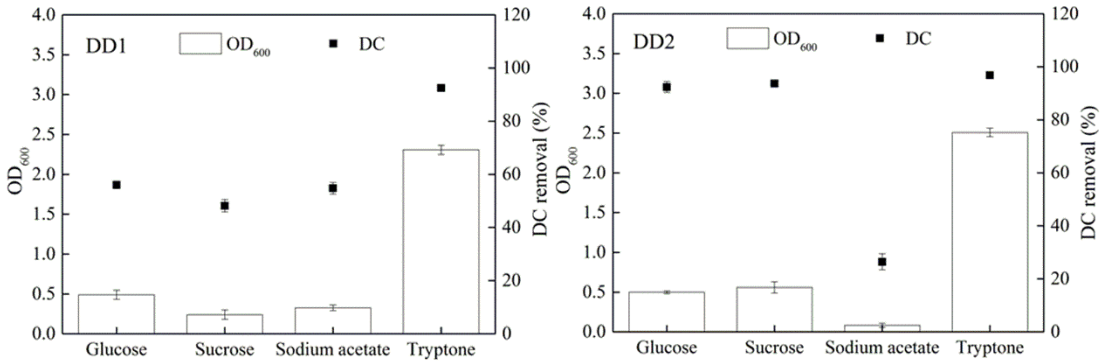

Figure S2. The OD_{600} readings and the DC removal percentages of DD1 and DD2 at the end of the degradation experiments (i.e., 7 days for DD1 and 2 days for DD2) with different substrates. The experimental conditions were identical to those in Figure 1, except that the concentrations for glucose, sucrose, sodium acetate, and tryptone were all set at 10 mg/L.

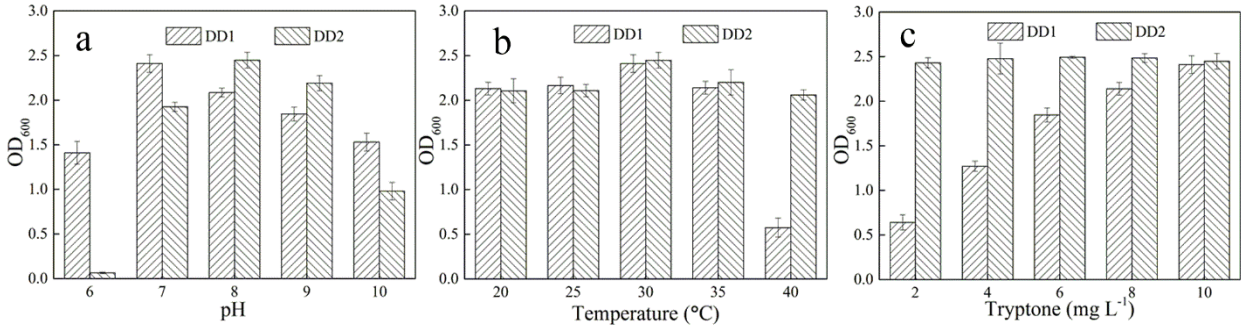

Figure S3. The OD_{600} of DD1 and DD2 at the end of the degradation experiments conducted under different (a) pHs, (b) temperatures, and (c) initial tryptone concentrations.

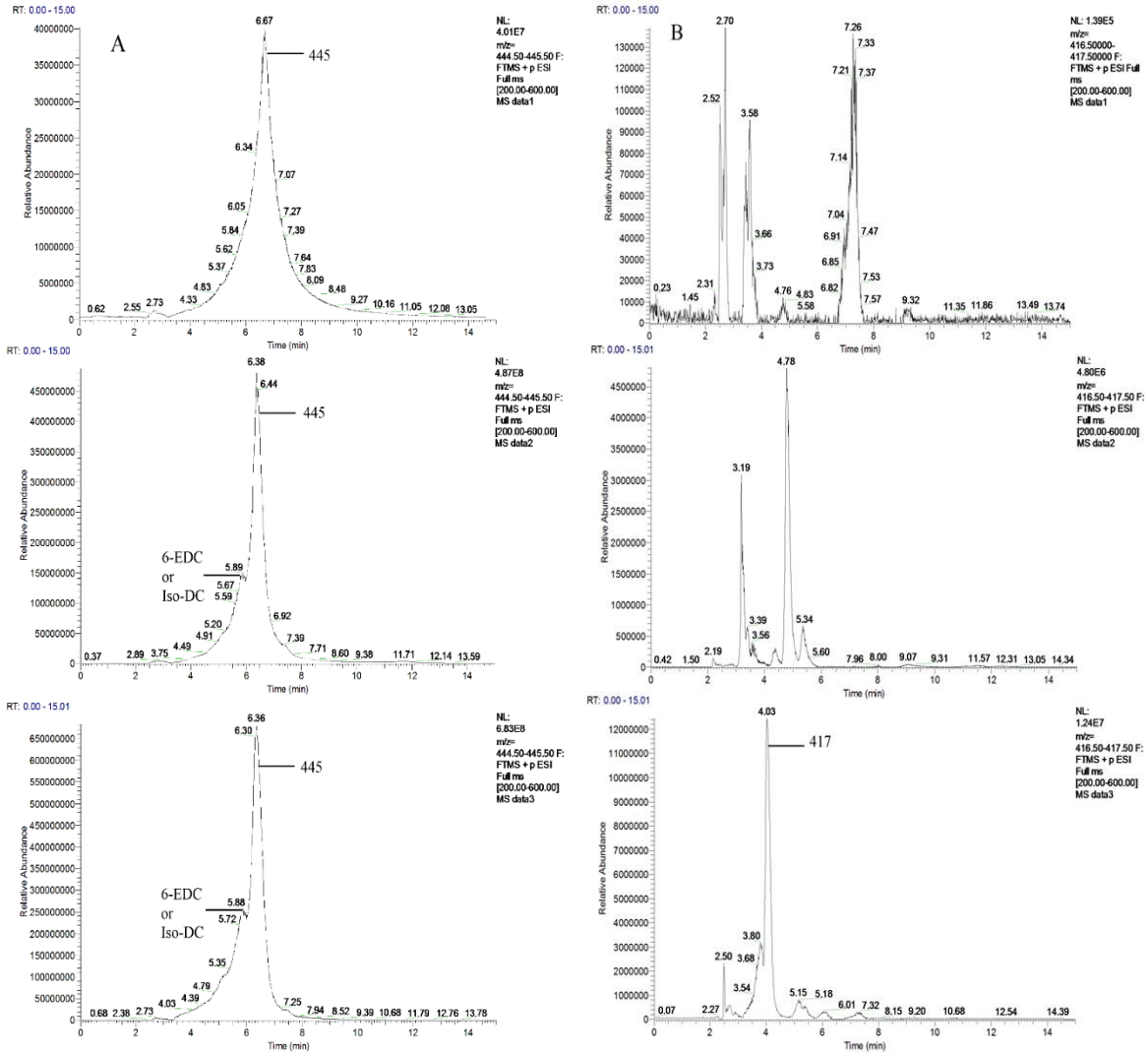
A
B
445
417
6-EDC
or
Iso-DC
Relative Abundance
Time (min)
RT: 0.00 - 15.00
RT: 0.00 - 15.01
NL:
4.01E7
m/z=
444.50-445.50 F:
FTMS + p ESI
Full ms
[200.00-600.00]
MS data1
NL: 1.39E5
m/z=
416.50000-
417.50000 F:
FTMS + p ESI Full
ms
[200.00-600.00]
MS data1
NL:
4.87E8
m/z=
444.50-445.50 F:
FTMS + p ESI
Full ms
[200.00-600.00]
MS data2
NL:
4.80E6
m/z=
416.50-417.50 F:
FTMS + p ESI
Full ms
[200.00-600.00]
MS data2
NL:
6.83E8
m/z=
444.50-445.50 F:
FTMS + p ESI
Full ms
[200.00-600.00]
MS data3
NL:
1.24E7
m/z=
416.50-417.50 F:
FTMS + p ESI
Full ms
[200.00-600.00]
MS data3

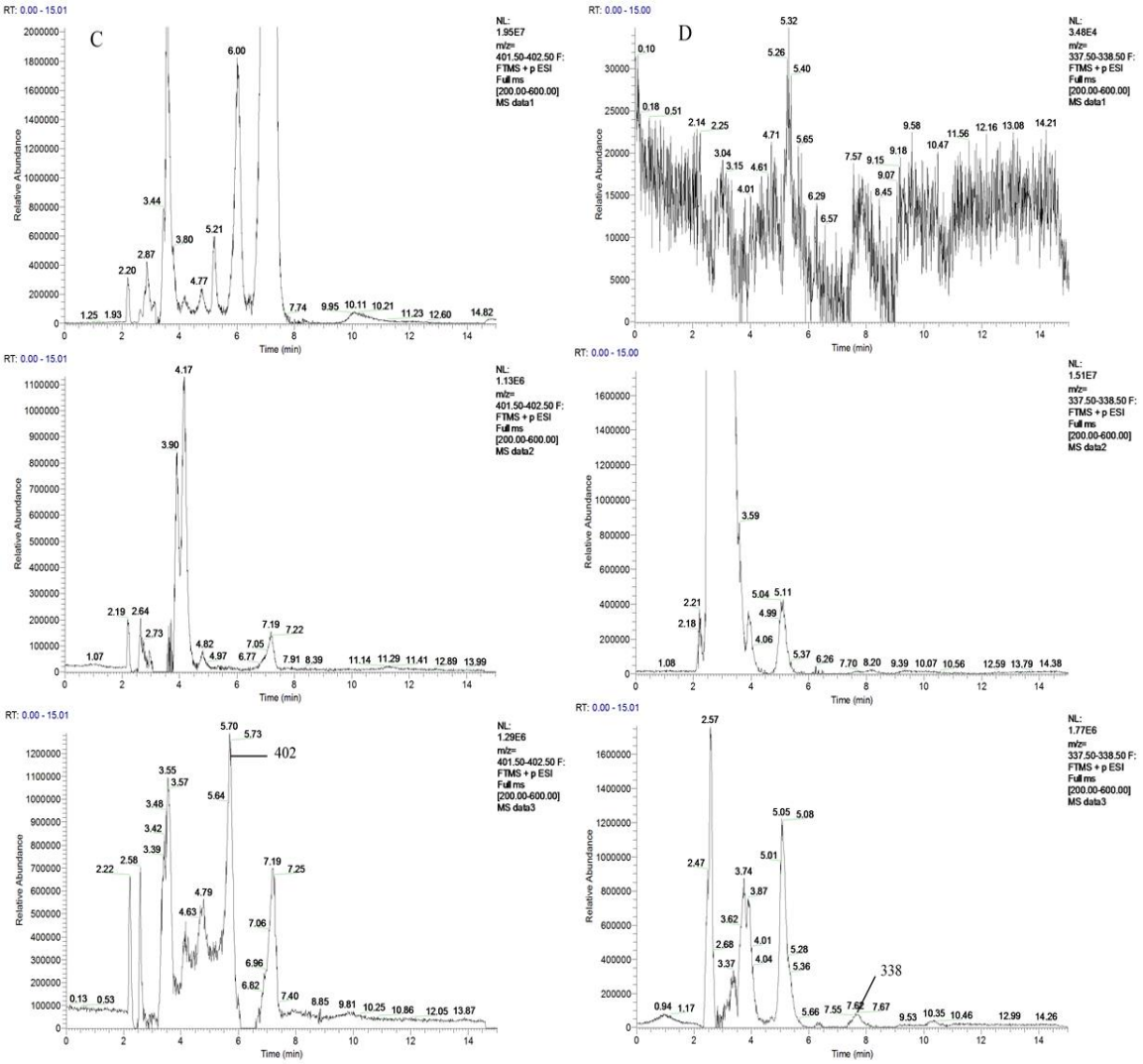
C
D
RT: 0.00 - 15.01
RT: 0.00 - 15.00
NL:
1.95E7
m/z=
401.50-402.50 F:
FTMS + p ESI
Full ms
[200.00-600.00]
MS data1
NL:
3.48E4
m/z=
337.50-338.50 F:
FTMS + p ESI
Full ms
[200.00-600.00]
MS data1
NL:
1.13E6
m/z=
401.50-402.50 F:
FTMS + p ESI
Full ms
[200.00-600.00]
MS data2
NL:
1.51E7
m/z=
337.50-338.50 F:
FTMS + p ESI
Full ms
[200.00-600.00]
MS data2
NL:
1.29E6
m/z=
401.50-402.50 F:
FTMS + p ESI
Full ms
[200.00-600.00]
MS data3
NL:
1.77E6
m/z=
337.50-338.50 F:
FTMS + p ESI
Full ms
[200.00-600.00]
MS data3
402
338
Relative Abundance
Time (min)

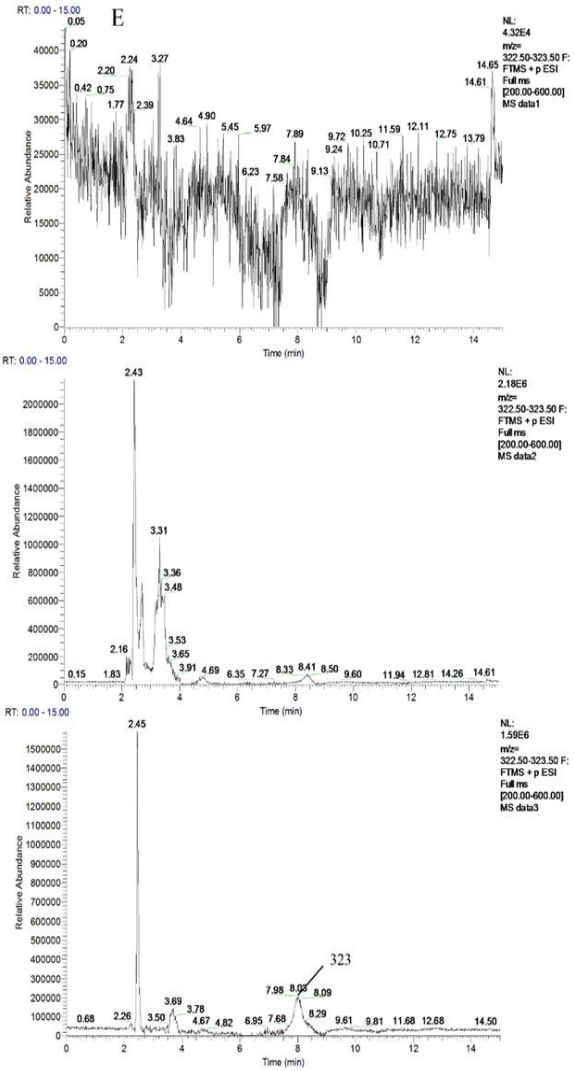

Figure S4. Extracted ion chromatograms at (A) m/z 445, (B) m/z 417, (C) m/z 402, (D) m/z 338, (E) m/z 323 from the degradation experiment of DD1. Within each panel, the subpanel from top to bottom represent initial DC parent compound on Day 0, degradation products from hydrolysis and biotransformation on Day 3. The peaks were identified using mass spectrometry.

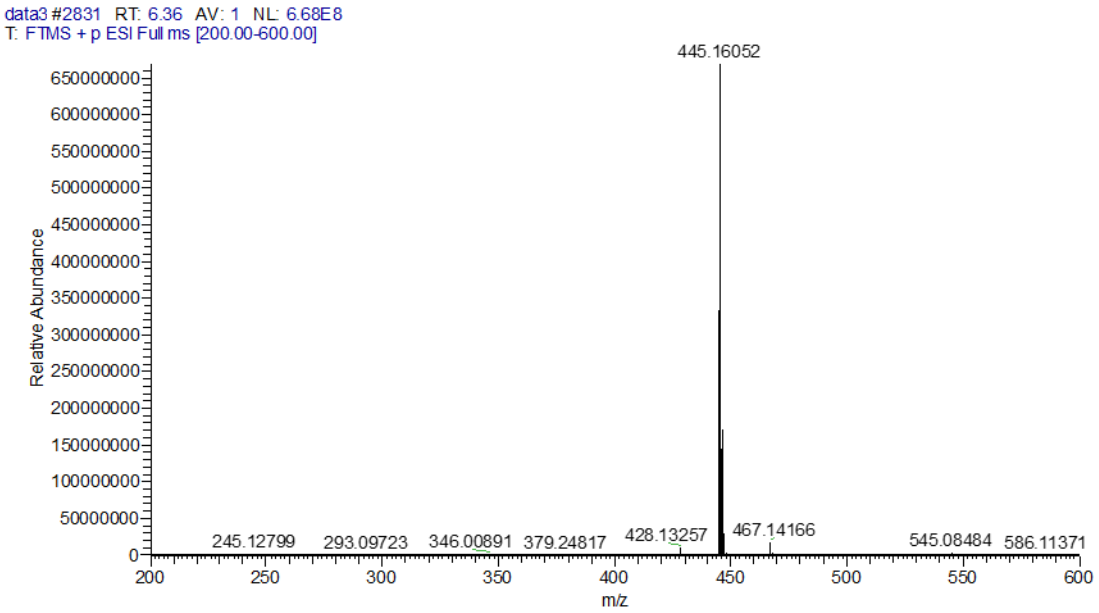

Figure S5. Mass spectrum of doxycycline (DC-445).

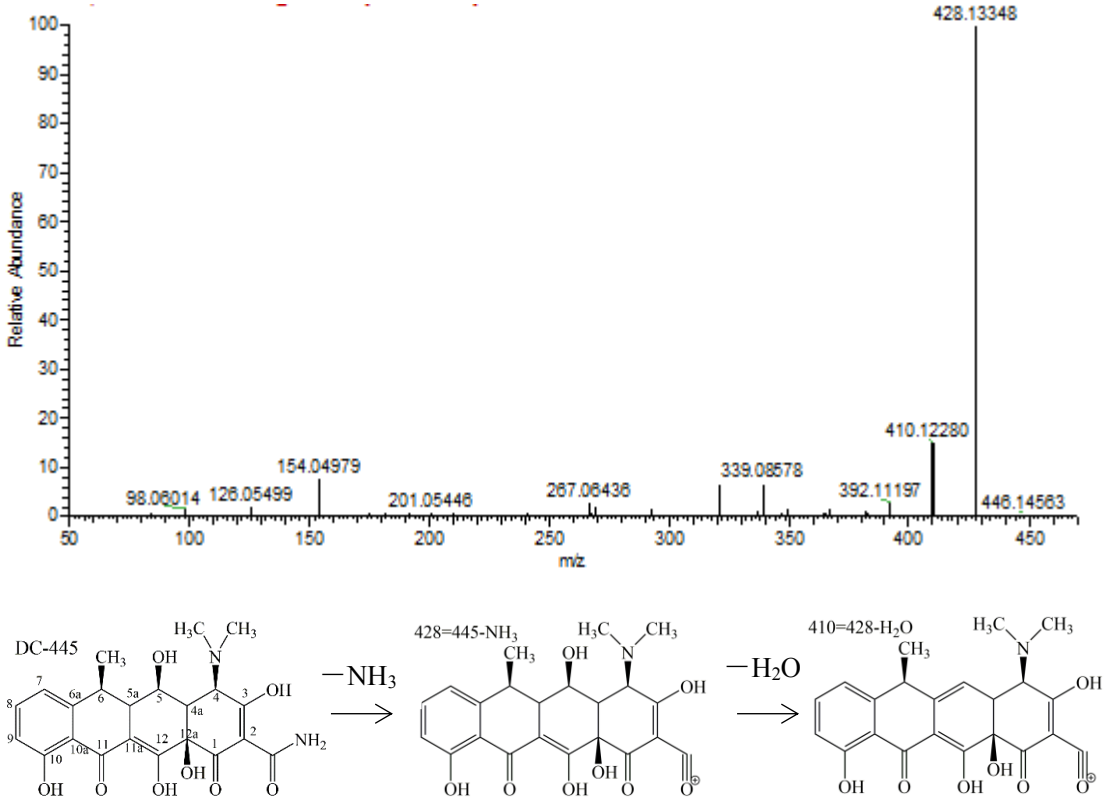

Figure S6. The secondary mass spectrometry (MS2) fragmentation profile and proposed fragmentation pattern of DC-445.

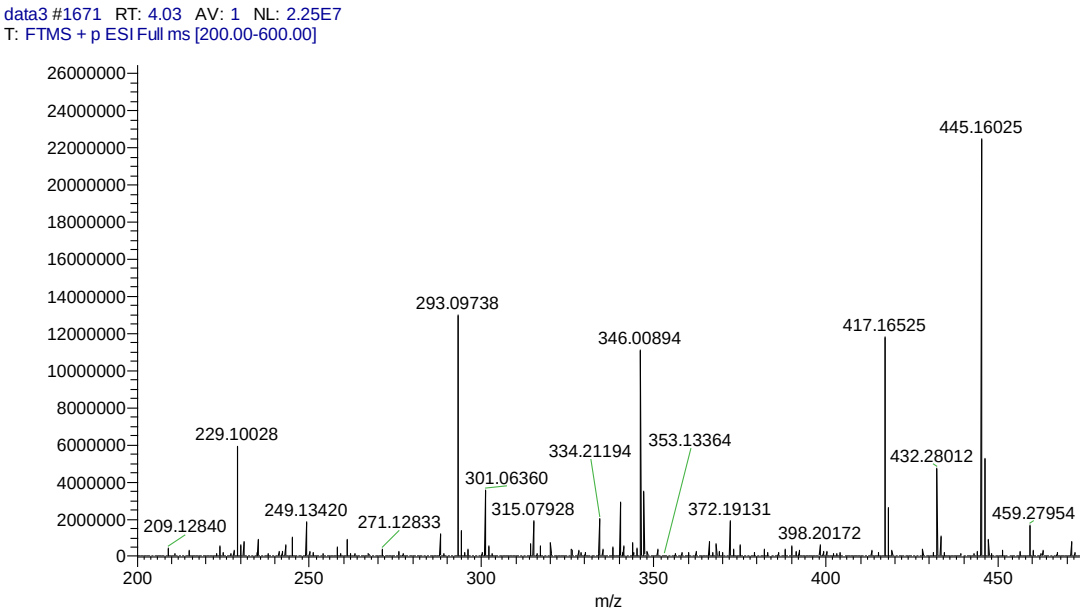

Figure S7. Mass spectrum of DP-417.

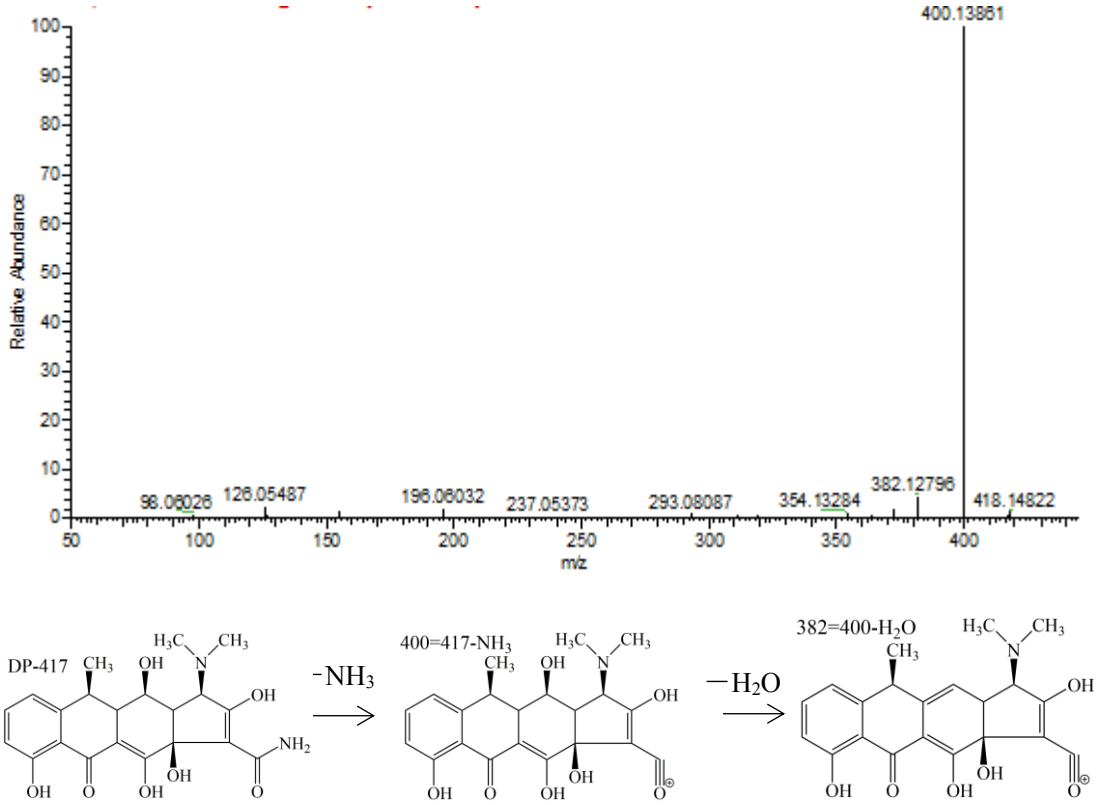

Figure S8. The MS2 fragmentation profile and proposed fragmentation pattern of DP-417.

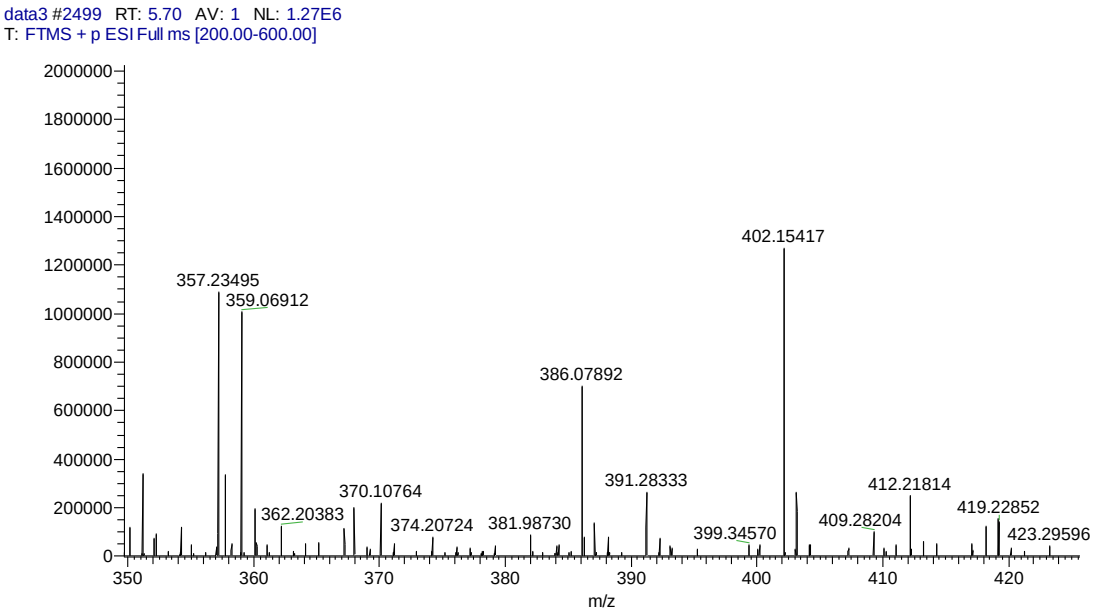

Figure S9. Mass spectrum of DP-402.

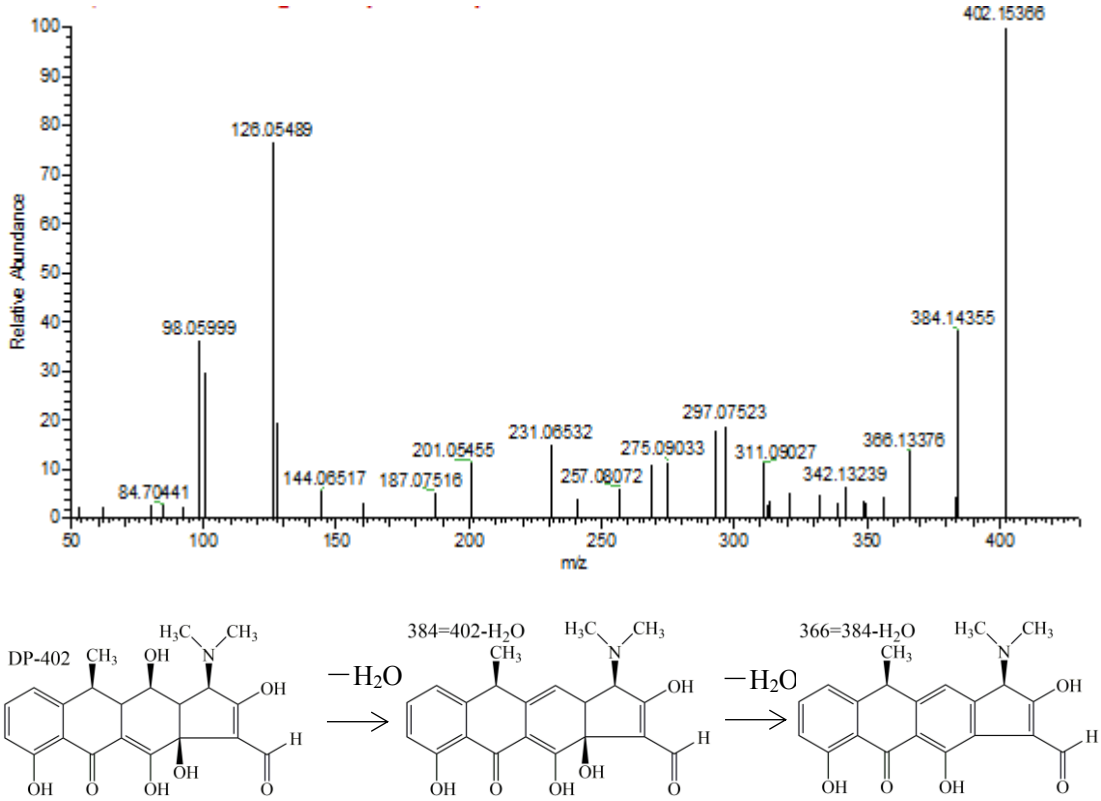

Figure S10. The MS2 fragmentation profile and proposed fragmentation pattern of DP-402.

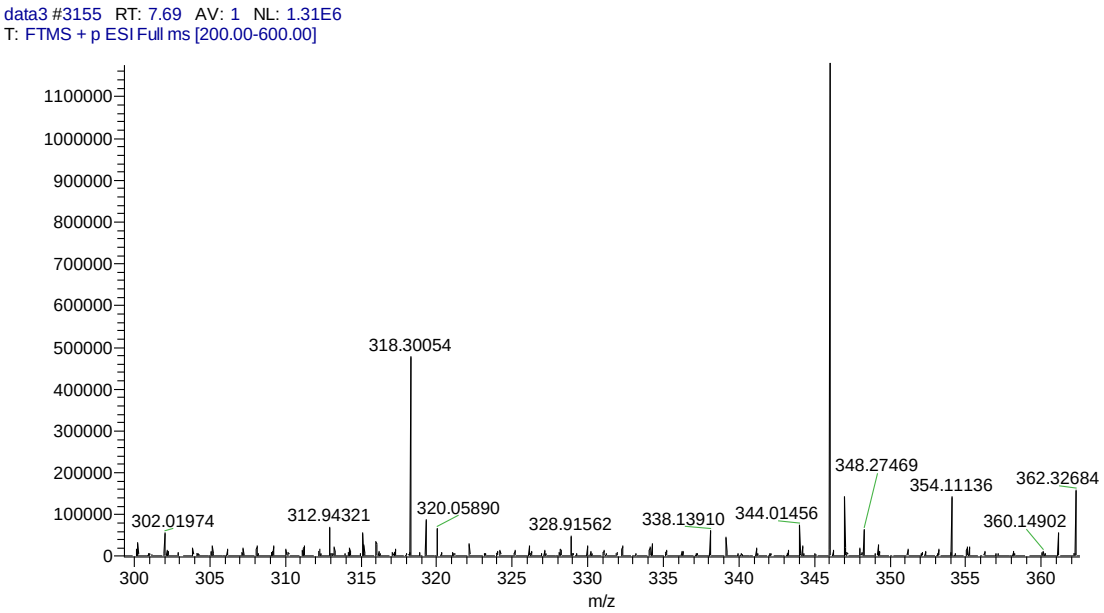

Figure S11. Mass spectrum of DP-338.

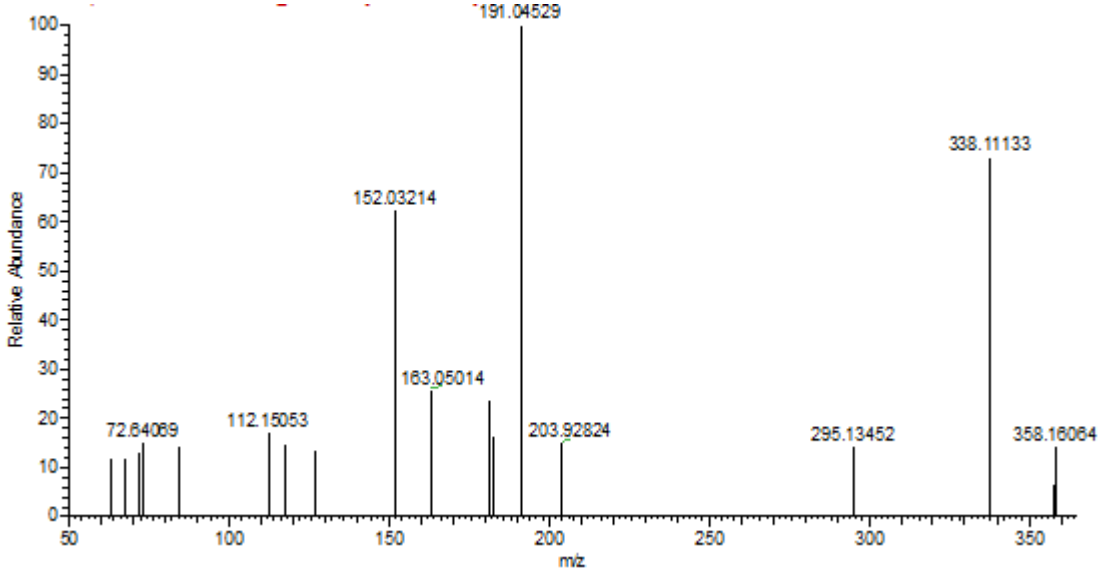

Figure S12. The MS2 fragmentation profile of DP-338.

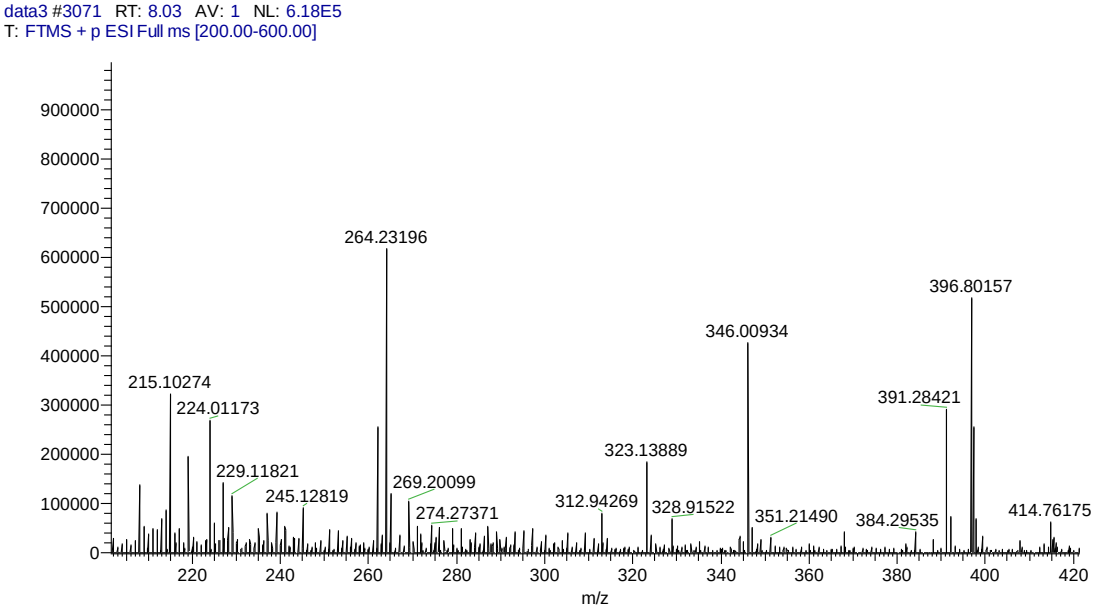

Figure S13. Mass spectrum of DP-323.

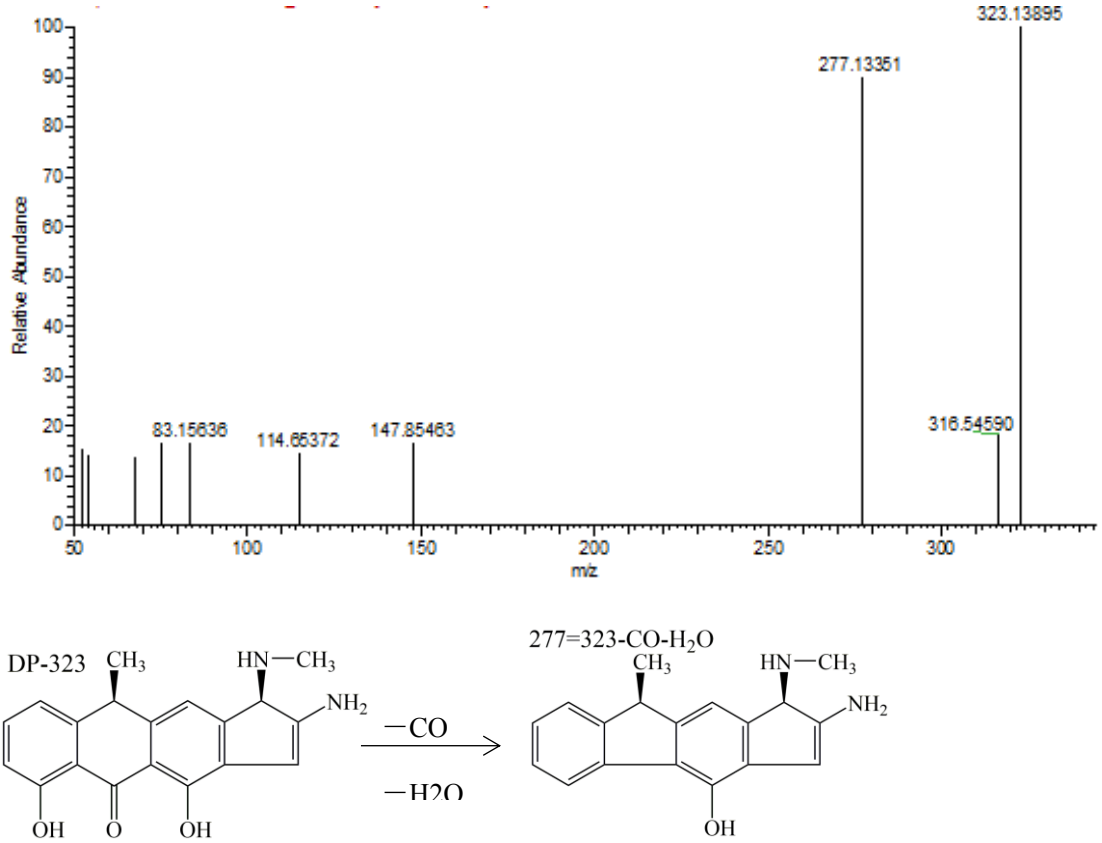

Figure S14. The MS2 fragmentation profile and proposed fragmentation pattern of DP-323.

Sphingobacterium mizutaii DD2

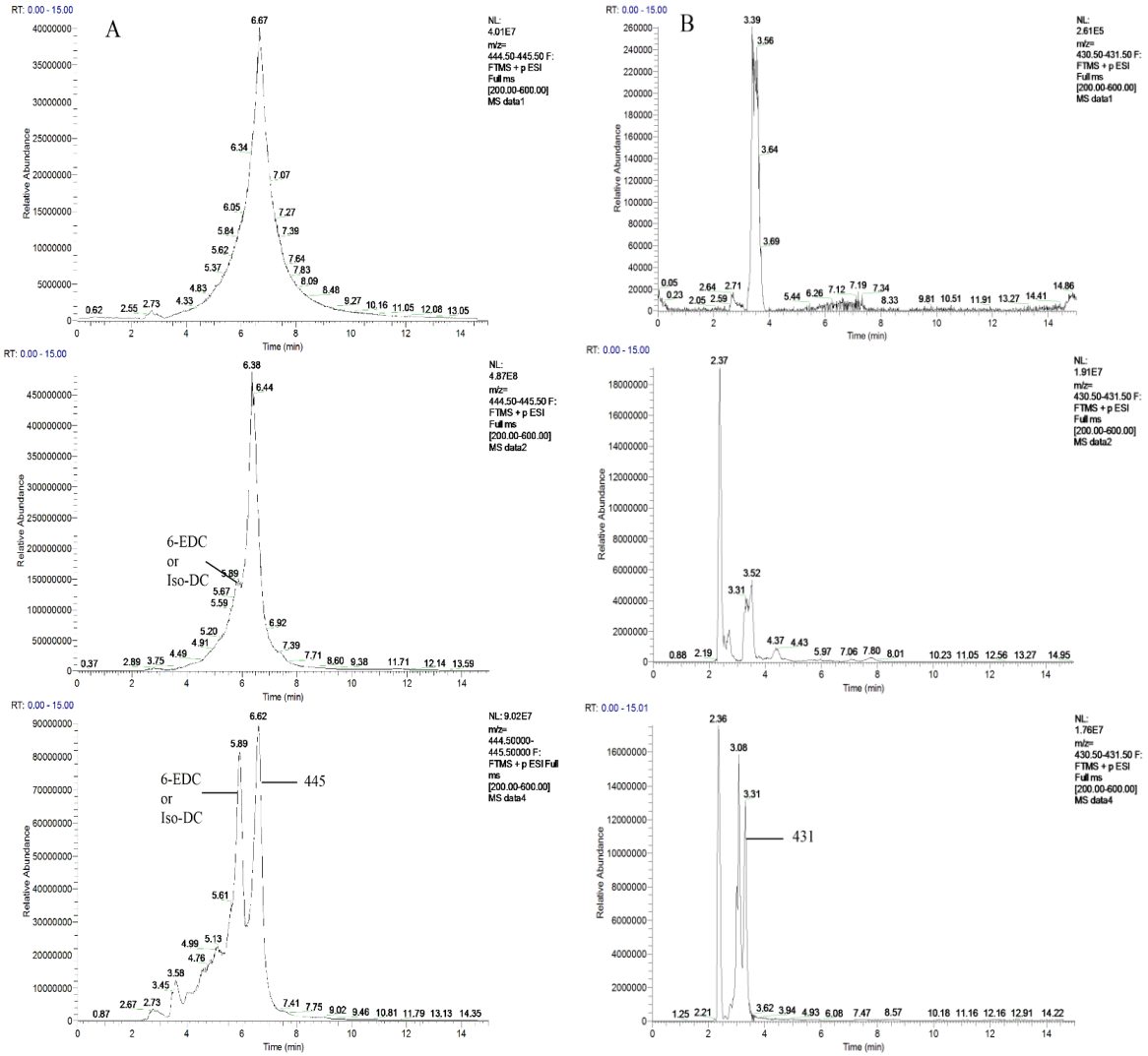

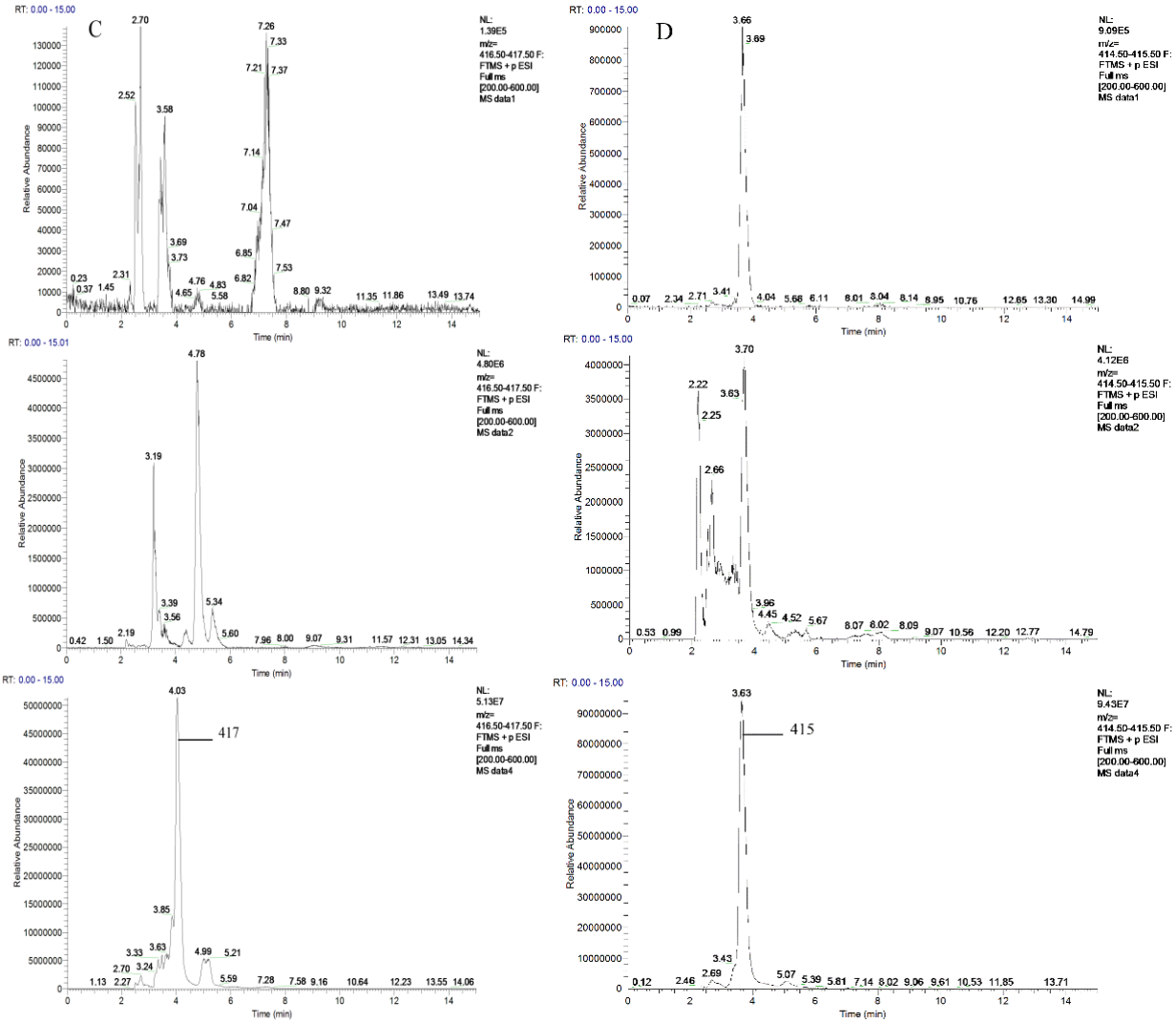
C
D
RT: 0.00 - 15.00
NL:
1.39E5
m/z=
416.50-417.50 F:
FTMS + p ESI
Full ms
[200.00-600.00]
MS data1
NL:
9.09E5
m/z=
414.50-415.50 F:
FTMS + p ESI
Full ms
[200.00-600.00]
MS data1
RT: 0.00 - 15.01
NL:
4.80E6
m/z=
416.50-417.50 F:
FTMS + p ESI
Full ms
[200.00-600.00]
MS data2
NL:
4.12E6
m/z=
414.50-415.50 F:
FTMS + p ESI
Full ms
[200.00-600.00]
MS data2
NL:
5.13E7
m/z=
416.50-417.50 F:
FTMS + p ESI
Full ms
[200.00-600.00]
MS data4
417
NL:
9.43E7
m/z=
414.50-415.50 F:
FTMS + p ESI
Full ms
[200.00-600.00]
MS data4
415
Relative Abundance
Time (min)

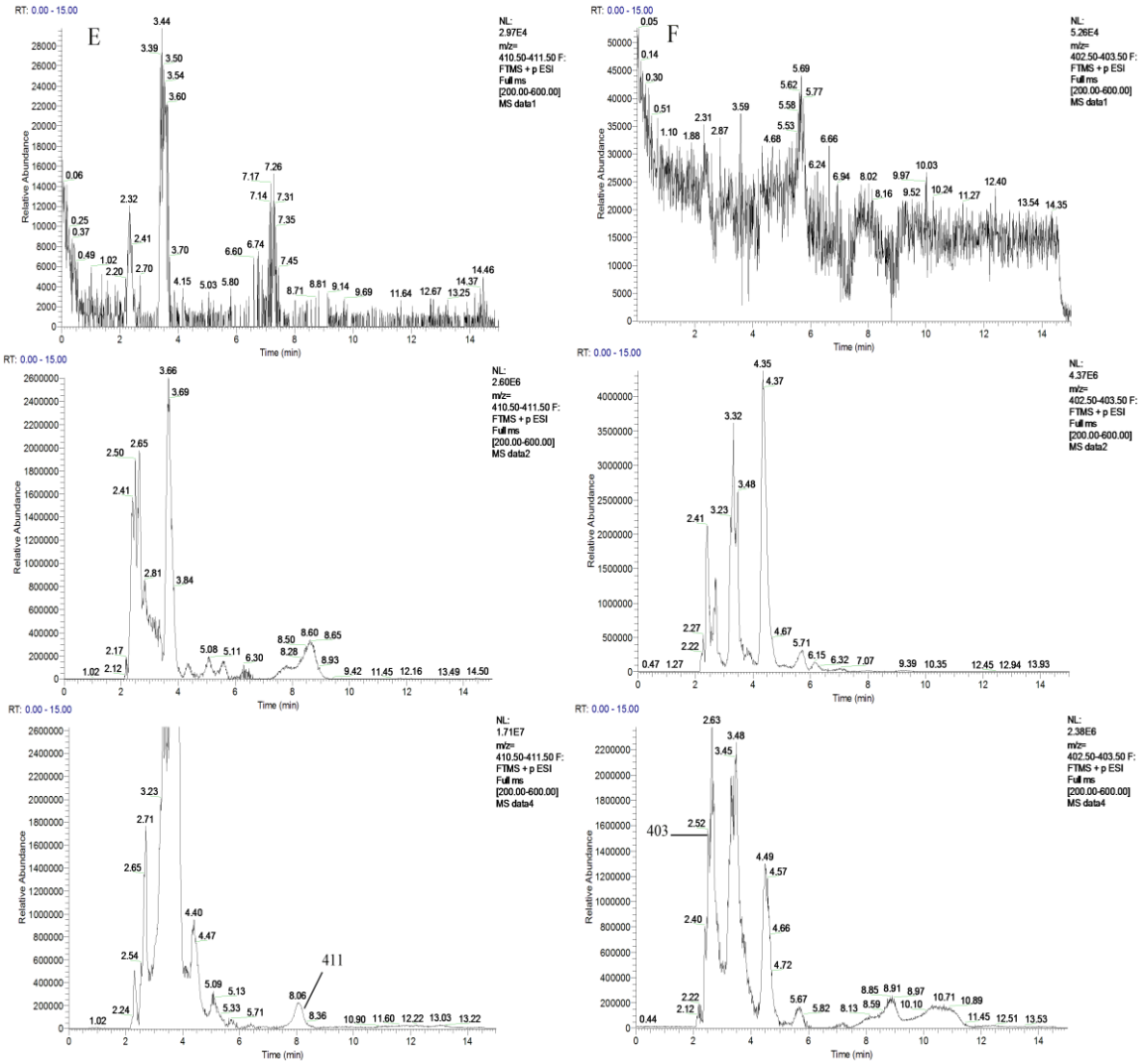
E
F
RT: 0.00 - 15.00
Relative Abundance
Time (min)
NL:
2.97E4
m/z=
410.50-411.50 F:
FTMS + p ESI
Full ms
[200.00-600.00]
MS data1
NL:
5.26E4
m/z=
402.50-403.50 F:
FTMS + p ESI
Full ms
[200.00-600.00]
MS data1
NL:
2.60E6
m/z=
410.50-411.50 F:
FTMS + p ESI
Full ms
[200.00-600.00]
MS data2
NL:
4.37E6
m/z=
402.50-403.50 F:
FTMS + p ESI
Full ms
[200.00-600.00]
MS data2
NL:
1.71E7
m/z=
410.50-411.50 F:
FTMS + p ESI
Full ms
[200.00-600.00]
MS data4
NL:
2.38E6
m/z=
402.50-403.50 F:
FTMS + p ESI
Full ms
[200.00-600.00]
MS data4
411
403

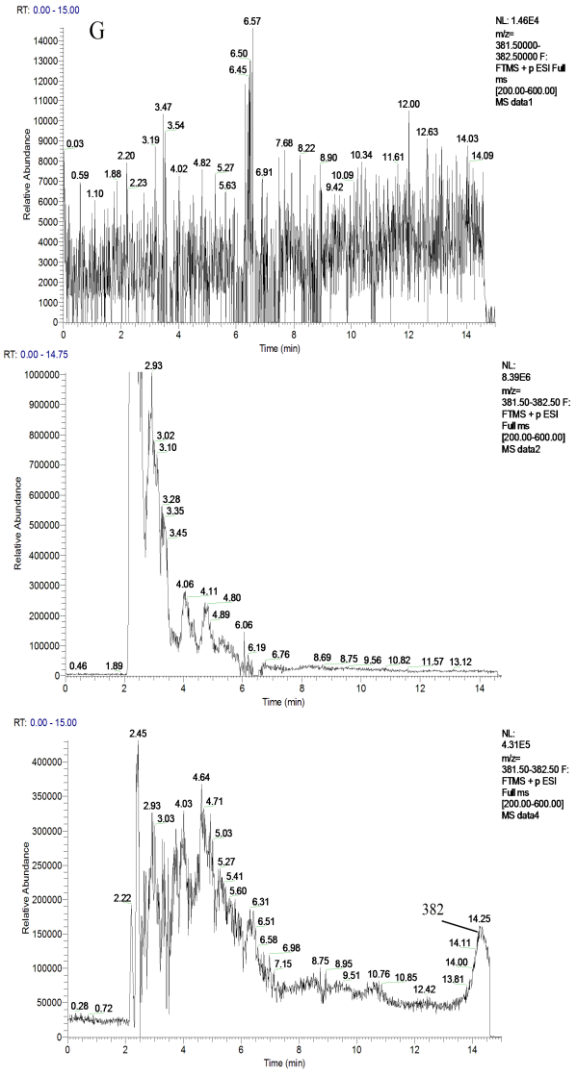

Figure S15. Extracted ion chromatograms at (A) m/z 445, (B) m/z 431, (C) m/z 417, (D) m/z 415, (E) m/z 411, (F) m/z 403, (G) m/z 382 from the degradation experiments of DD2. Within each panel, the ion chromatograms from top to bottom represent initial DC parent compound on Day 0, degradation products from hydrolysis and from biotransformation on Day 3. The peaks were identified using mass spectrometry.

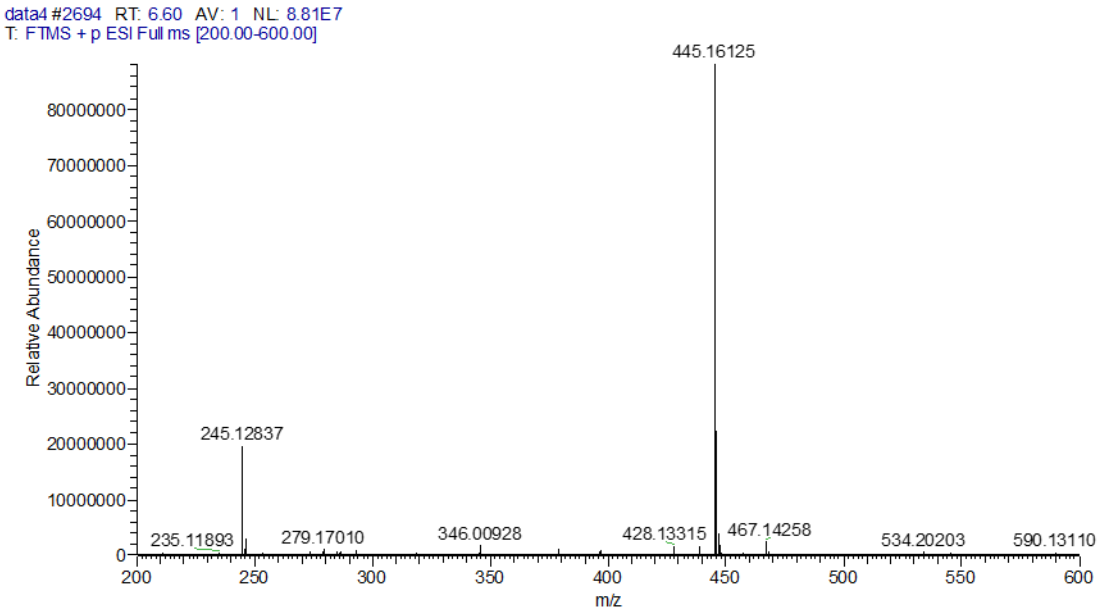

Figure S16. Mass spectrum of doxycycline.

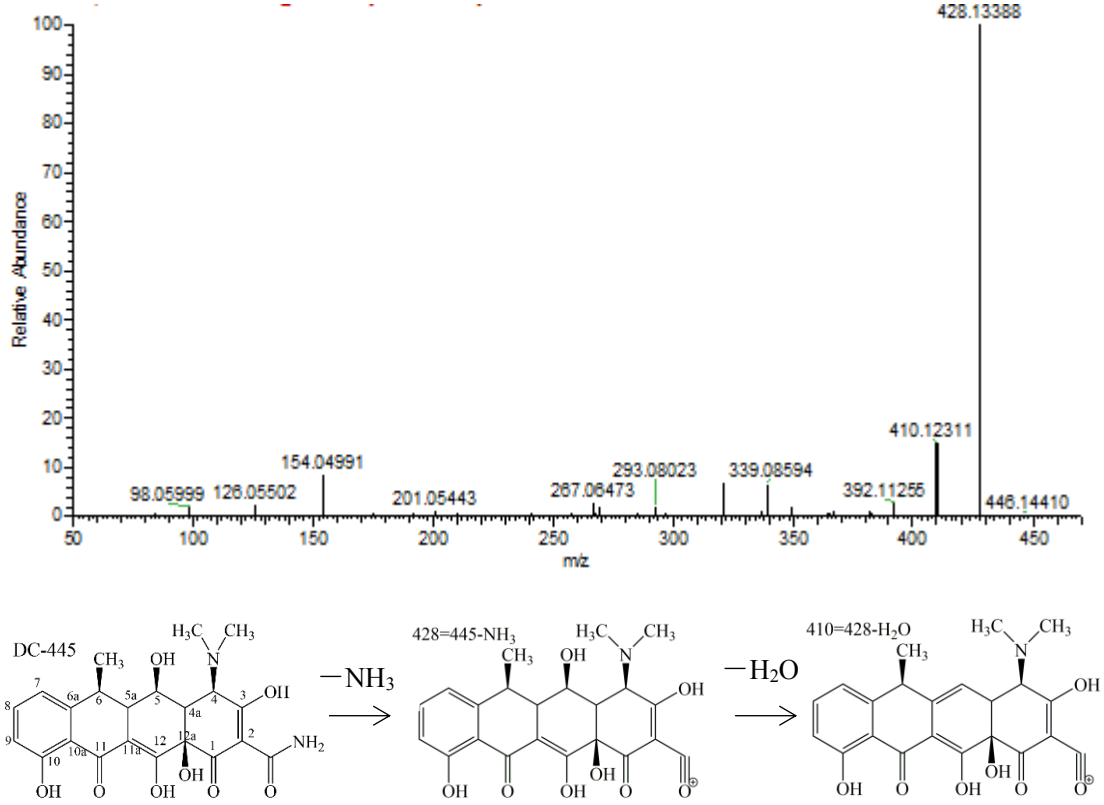

Figure S17. The MS2 fragmentation profile and proposed fragmentation pattern of DC-445.

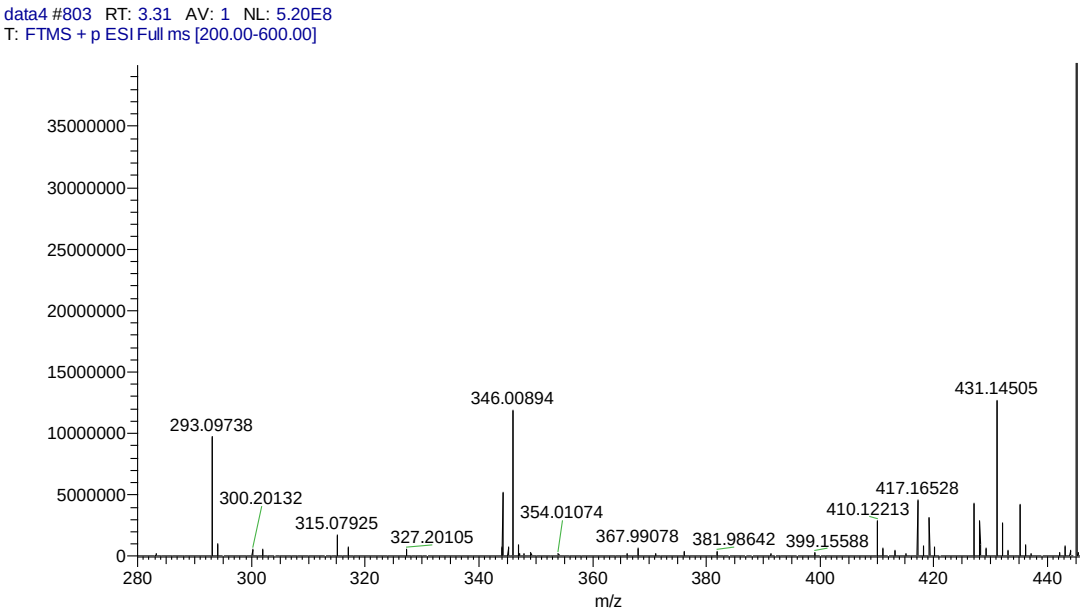

Figure S18. Mass spectrum of DP-431.

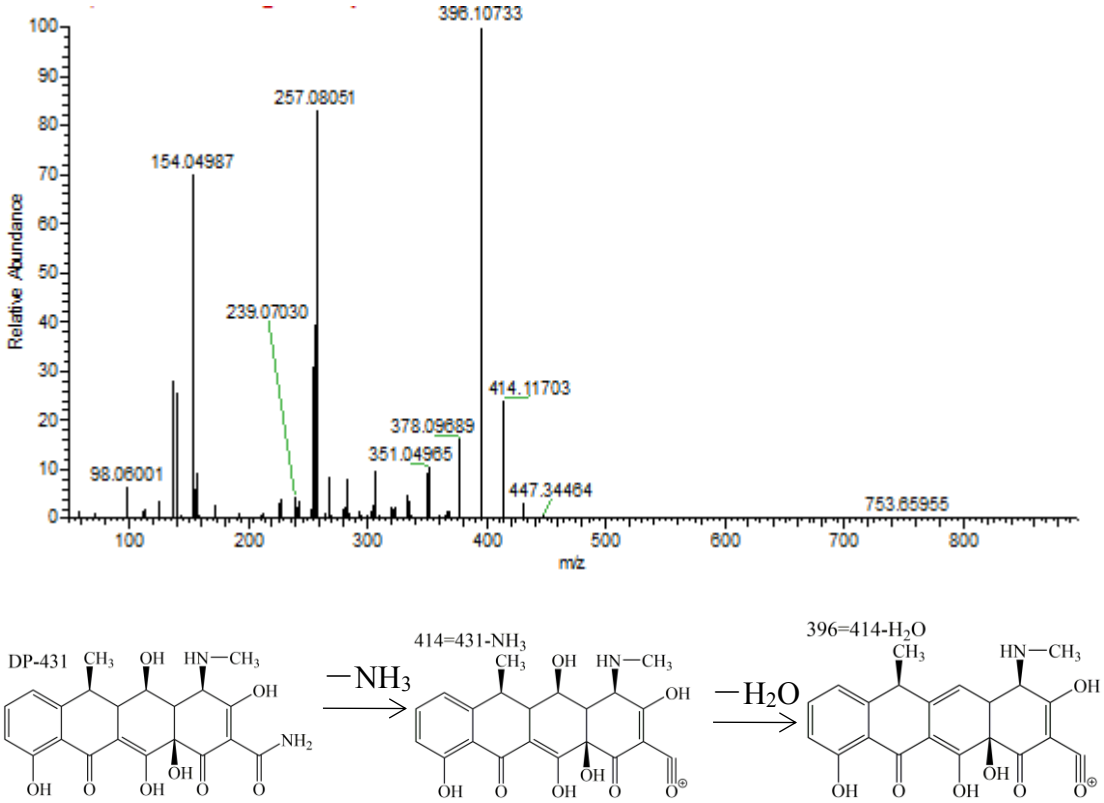

Figure S19. The MS2 fragmentation profile and proposed fragmentation pattern of DP-431.

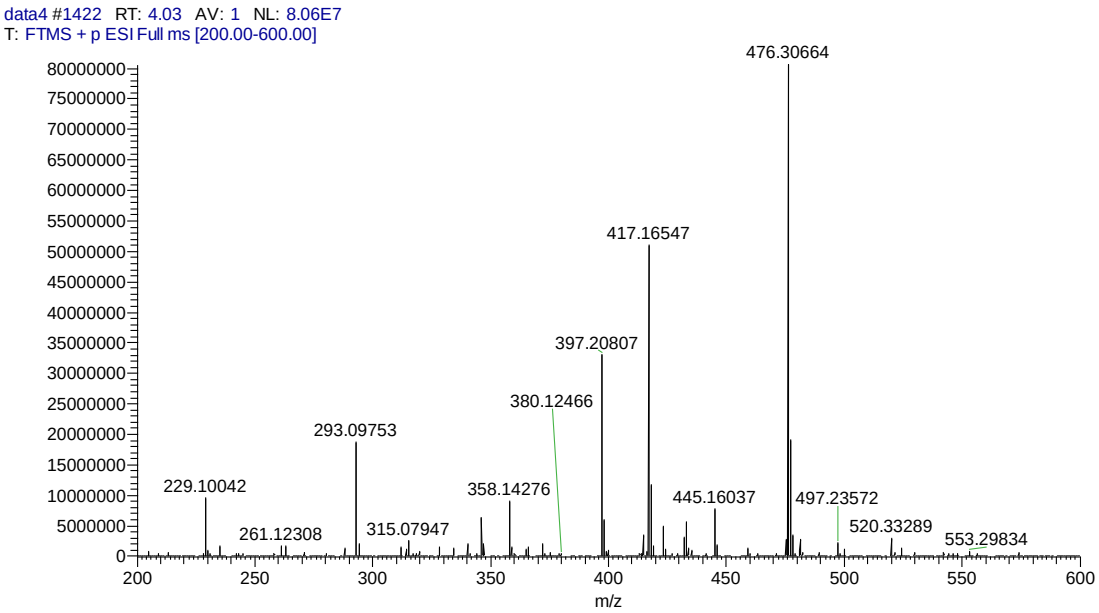

Figure S20. Mass spectrum of DP-417.

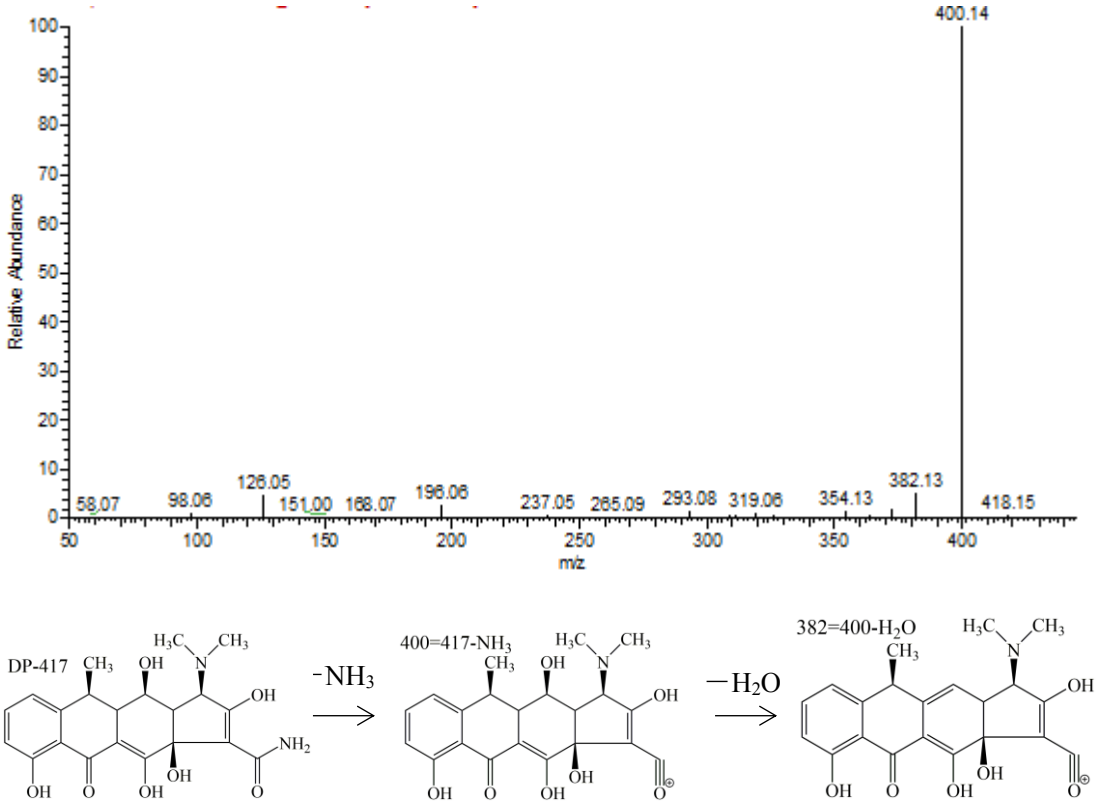

Figure S21. The MS2 fragmentation profile and proposed fragmentation pattern of DP-417.

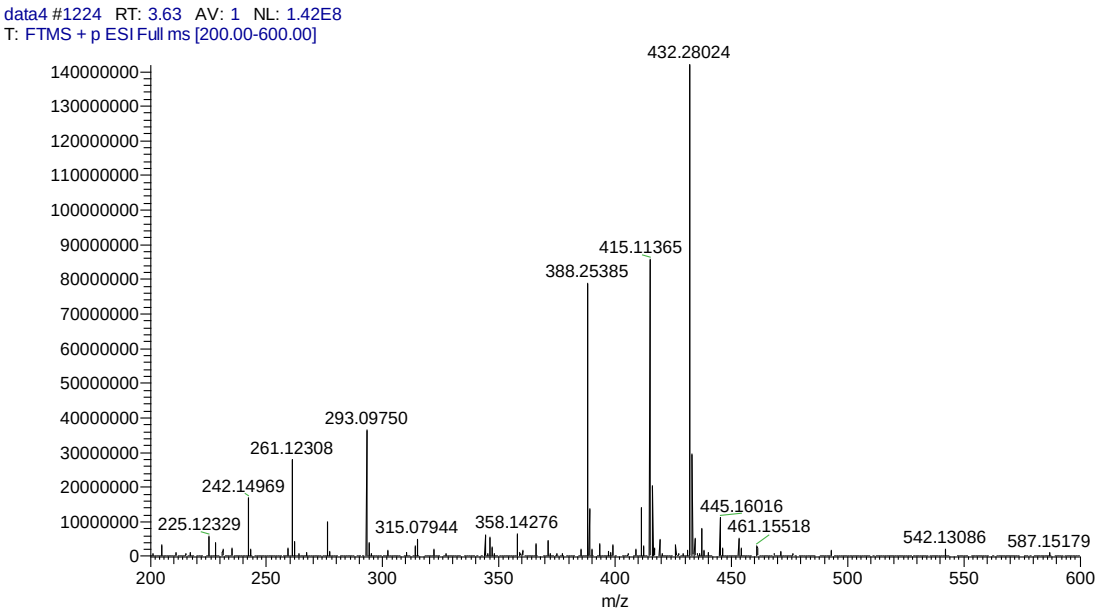

Figure S22. Mass spectrum of DP-415

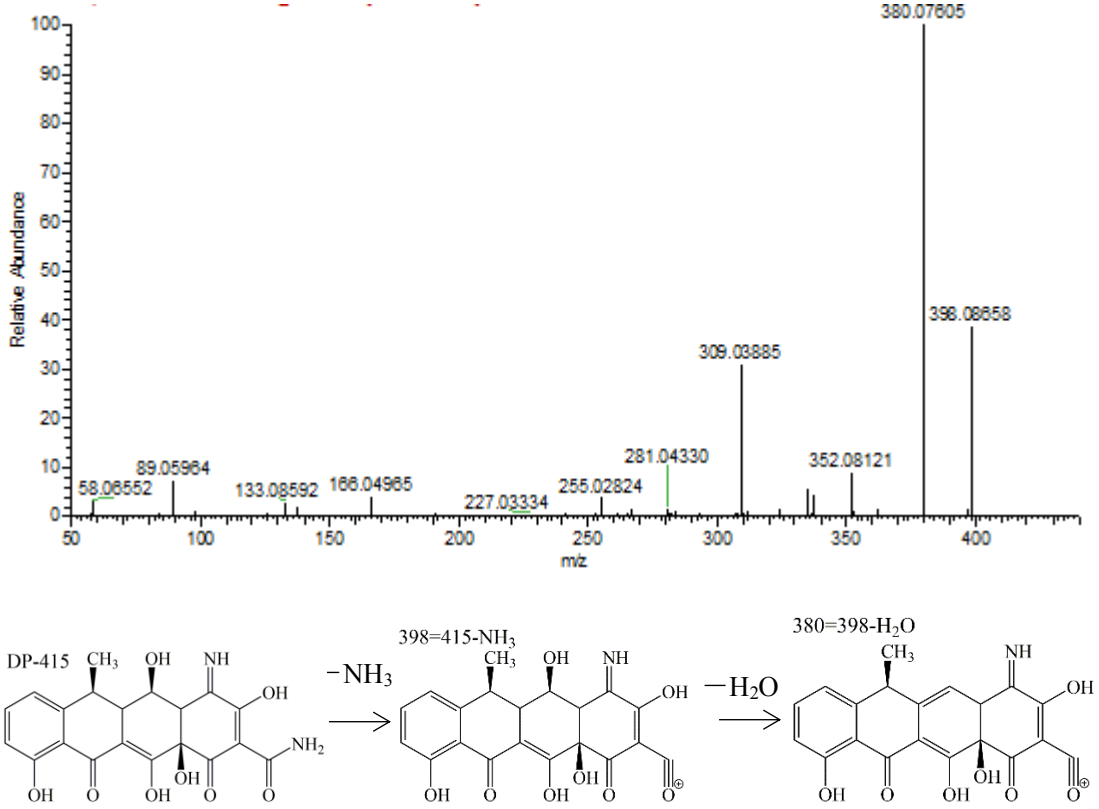

Figure S23. The MS2 fragmentation profile and proposed fragmentation pattern of DP-415.

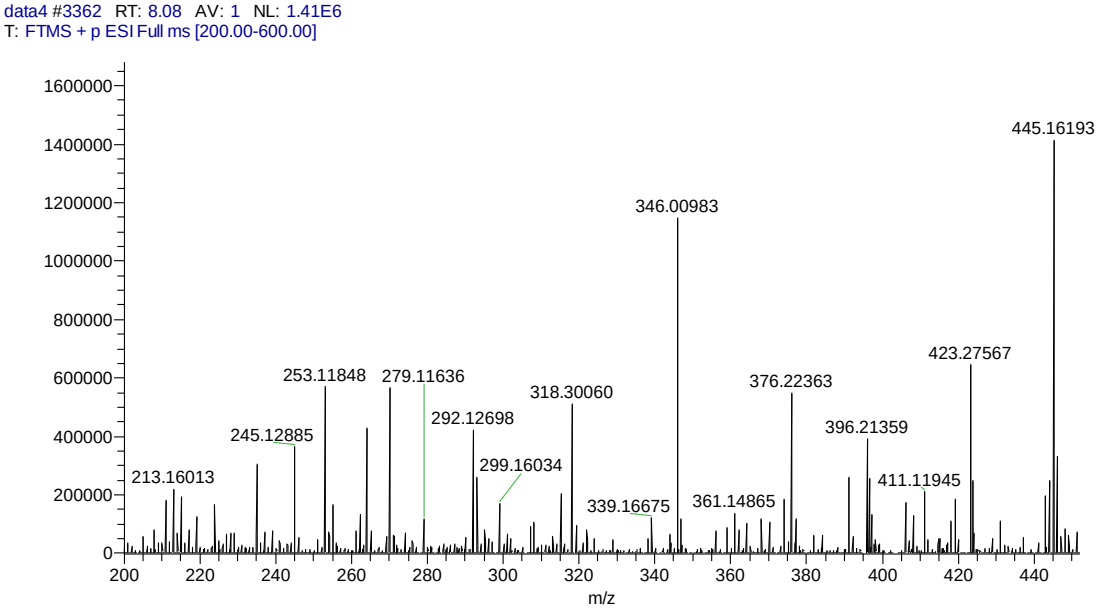

Figure S24. Mass spectrum of DP-411.

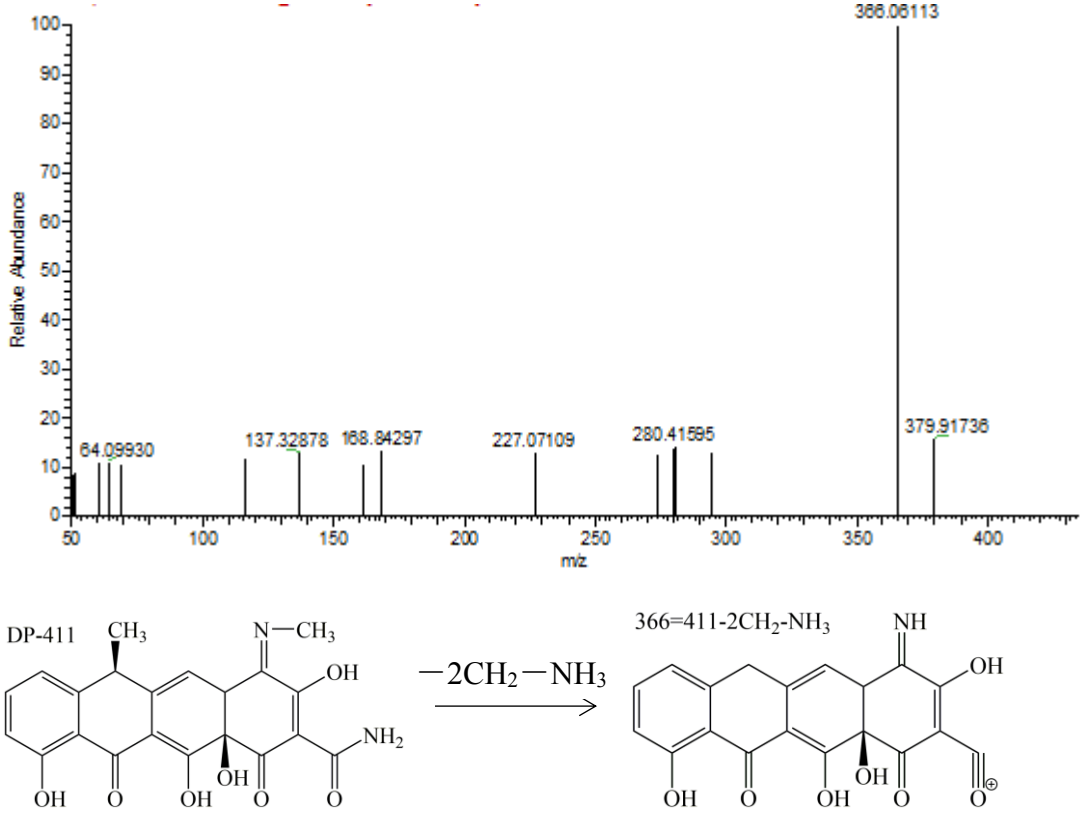

Figure S25. The MS2 fragmentation profile and proposed fragmentation pattern of DP-411.

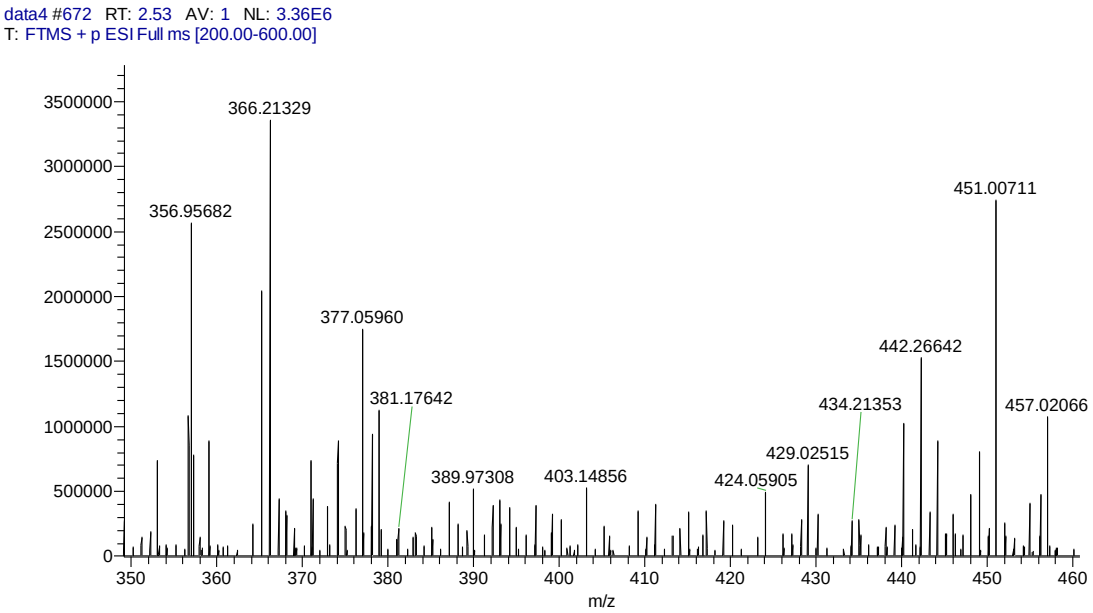

Figure S26. Mass spectrum of DP-403.

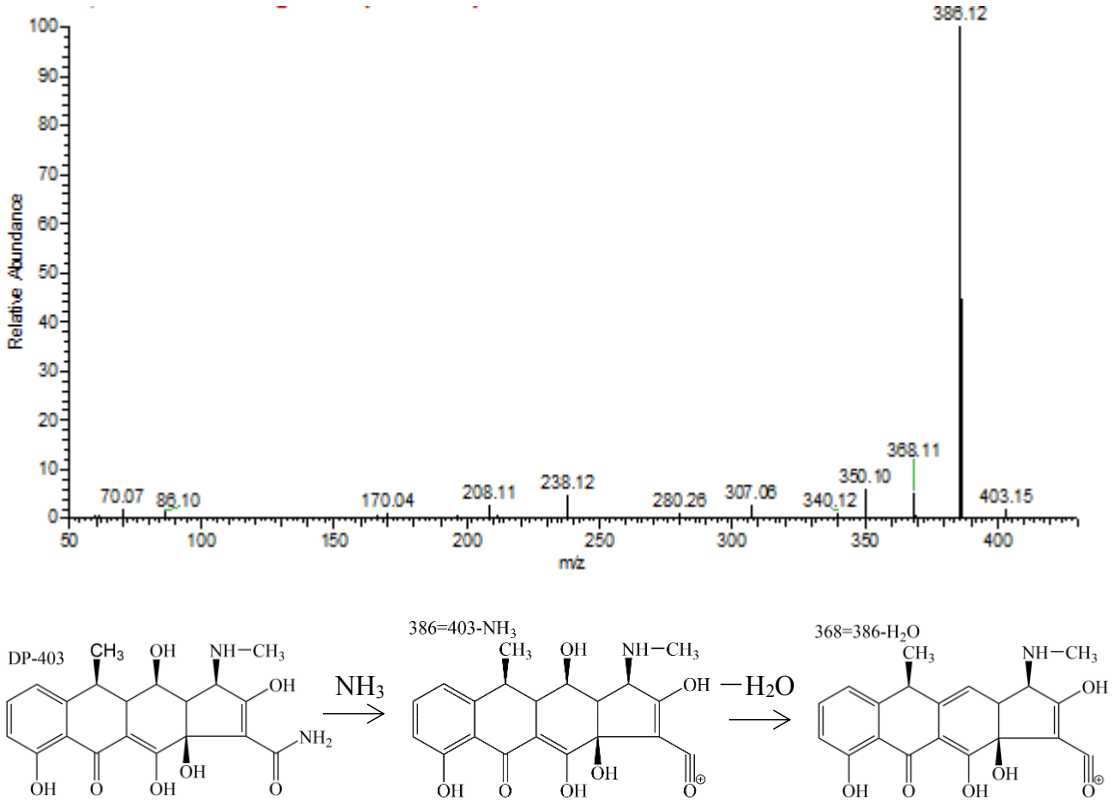

Figure S27. The MS2 fragmentation profile and proposed fragmentation pattern of DP-403.

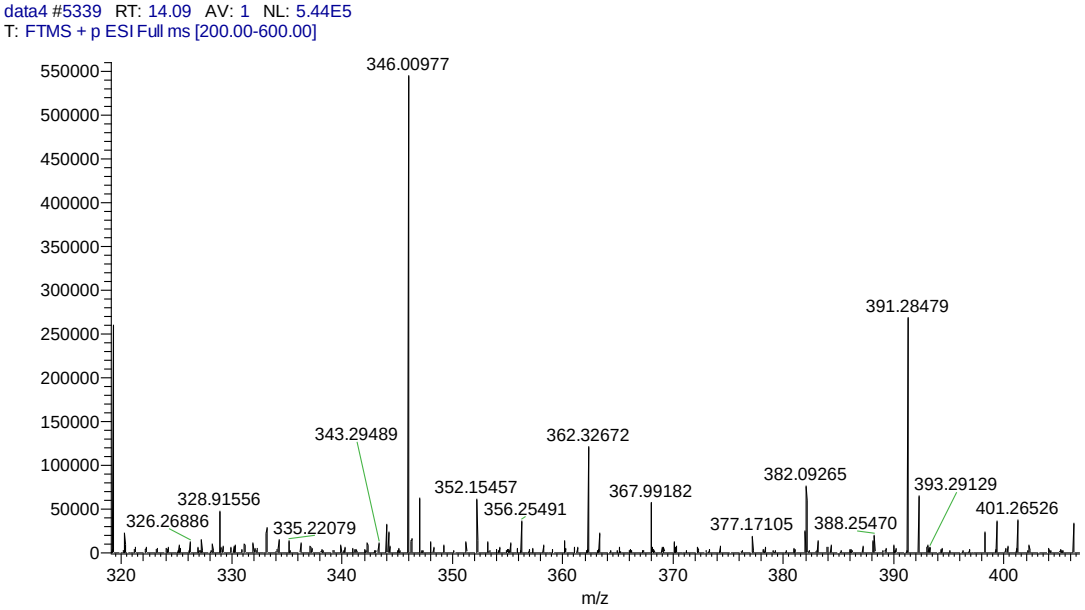

Figure S28. Mass spectrum of DP-382.

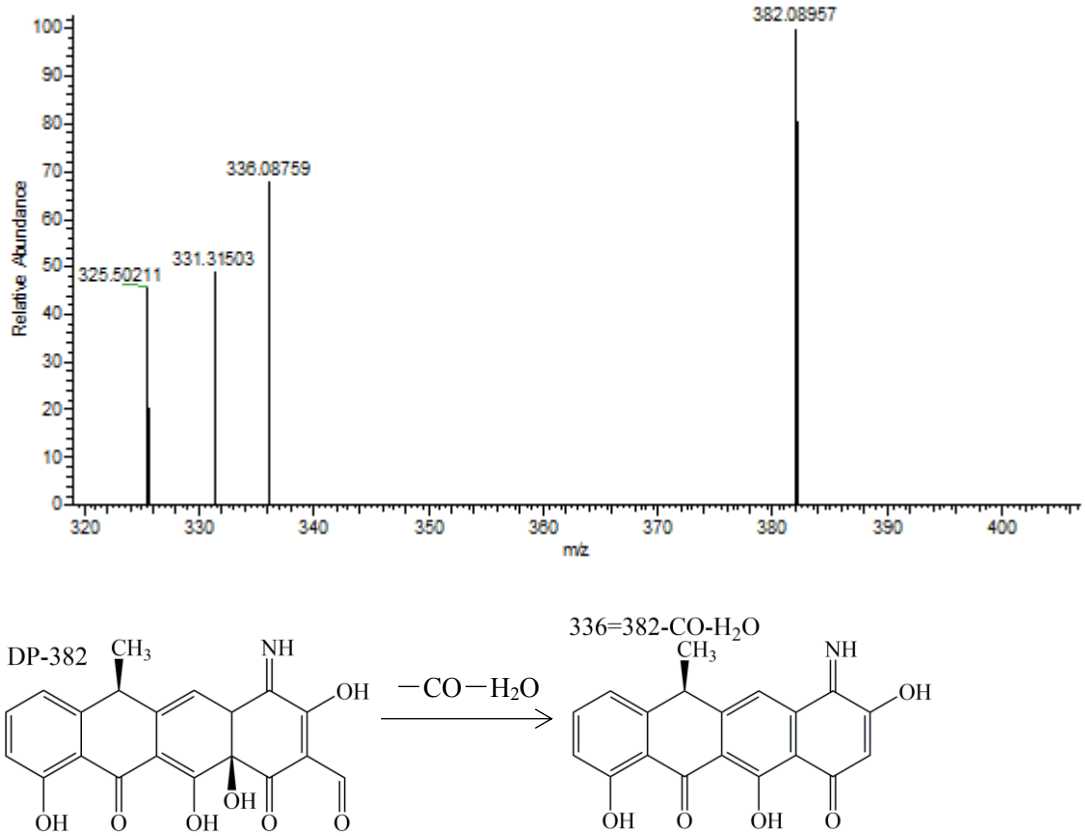

Figure S29. The MS2 fragmentation profile and proposed fragmentation pattern of DP-382.